BAR-ILAN UNIVERSITY

Extraordinary Hall effect in $SrRuO_3$

YEVGENY KATS

Submitted in partial fulfillment of the requirements for the Master's degree in the Department of Physics, Bar-Ilan University.

Ramat-Gan, Israel 2004

This work was carried out under the supervision of

Professor Lior Klein

Department of Physics

Bar-Ilan University

Acknowledgments

First, I would like to thank my advisor, Prof. Lior Klein, who introduced me into experimental solid state physics, gave me an opportunity to be involved in every aspect of a research work, and supported and promoted me in many ways during the wonderful years of my work with him. I highly appreciate his great dedication to his students.

I also want to thank Isaschar Genish, a person with amazing experimental skills, who worked on his thesis in parallel with me, and contributed much to the work presented here.

I would like to thank Jim Reiner from the KGB group at Stanford, who made his excellent samples of $SrRuO_3$ available to us, and worked together with us on several experiments which are not described here. I am also grateful to the other members of the KGB group with whom I worked during my visits there, particularly, Nadya Mason and Gertjan Koster.

I am thankful to John M. Densmore and Gokul Gopalakrishnan for a careful proofreading of parts of this text.

I appreciate the help of Prof. Haim Taitelbaum, who has been the Head of the Physics Department during most of this period, whose strong support gave me the possibility to pursue the M. Sc. studies in parallel with my army service.

It has been a great pleasure for me to share the lab with Shahar Levy, Michael Feigenson, Isaschar Genish, Yosi Bason, and Moty Schultz.

Finally, I want to thank my family, who helped me and supported me all the way.

Contents

Abstract

While the extraordinary Hall effect (EHE) has been known for more than a century, there is still no consensus regarding the importance of the various factors which may be responsible for this effect in different materials. Particularly, a new type of models (relating the EHE to the Berry phase effect in the crystal momentum space) has been intensively discussed in the last several years. The topics of this thesis are centered around the EHE in the itinerant ferromagnet $SrRuO_3$. This material has drawn much attention in the last years due to its unusual properties, which in some cases were interesting for themselves, and in other cases provided a convenient playground for investigating general material properties.

In order to explore the EHE in $SrRuO_3$, we needed to understand and investigate the anisotropy of the paramagnetic susceptibility in $SrRuO_3$ and the connection between magnetoresistance and magnetization. The work on these issues yielded results which are interesting and important even beyond their contribution to the understanding of the EHE in $SrRuO_3$, and they are also described in this thesis.

In Chapter 1 we provide an introduction to the EHE, and give an overview of the material properties of $SrRuO_3$. In Chapter 2 we give general experimental details. Chapter 3 describes an experiment in which we probe the magnetization-dependence of the EHE by performing measurements as a function of the magnetic field. By this

experiment we refute the recently suggested explanation for the strange behavior of the EHE in $SrRuO_3$ in terms of the Berry phase model. In Chapter 4 we explore the EHE of $SrRuO_3$ in the paramagnetic state. This experiment also reveals a strikingly large anisotropy in the paramagnetic susceptibility of $SrRuO_3$, which can be measured over a wide range of temperatures by using the EHE. Chapter 5 presents evidence for a non-trivial dependence of the EHE on the direction of the magnetization. Chapter 6 summarizes the main results. In Appendix A we establish a simple relation between the magnetic resistivity and the magnetization in $SrRuO_3$, which allows us to investigate the magnetic critical behavior by measurements of resistivity. The results of this Appendix have relevance to several methods and conclusions from the main text.

Chapter 1

Background

1.1 Extraordinary Hall effect (EHE)

Ordinary Hall effect (OHE)

Hall effect appears when a sample carrying an electric current I lies in magnetic field $\mathbf{B}$. The Lorentz force deflects the charge carriers, creating an excess surface charge on the sides of the sample. This charge produces a transverse electric field $\mathbf{E}_H$ in the sample given by

$$\mathbf{E}_H = -R_0 \mathbf{J} \times \mathbf{B}, \tag{1.1}$$

where $\mathbf{J}$ is the current density ($J = I/A$, where A is the sample cross-section area), and $R_0 = -1/ne$ is the Hall coefficient (n is the charge carrier density). Consequently, a transverse voltage V_H is created. In the measurement configuration depicted in Fig.

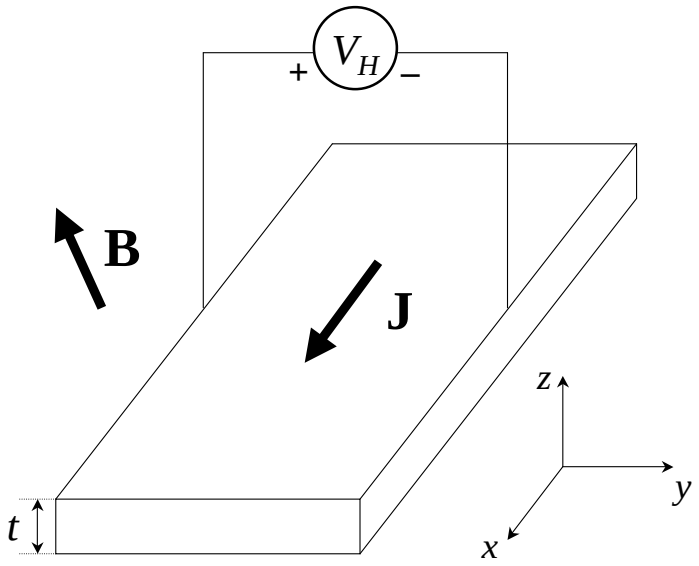

Figure 1.1: Hall effect measurement configuration.

1.1, the "Hall resistance" $R_H = V_H/I$ is given by

$$R_H = \frac{R_0 B_z}{t}. \tag{1.2}$$

The Hall effect can be also written in terms of the transverse resistivity $\rho_{xy} = E_y/J_x$ as

$$\rho_{xy} = R_0 B_z. \tag{1.3}$$

Extraordinary Hall effect (EHE)

In magnetic materials the Hall effect includes, in addition to the ordinary Hall effect (OHE), an "extraordinary" (or "anomalous") Hall effect (EHE), which depends on the magnetization $\mathbf{M}$. (The contribution of $\mathbf{M}$ to the OHE through the relation $\mathbf{B} = \mathbf{H} + \mu_0\mathbf{M}$ is usually much smaller than the EHE, and many times cancelled altogether due to the demagnetization effect.)

Commonly the EHE has been attributed to spin-dependent scattering and described as:

$$\rho_{xy}^{EHE} = R_s(\rho)\mu_0 M\, \hat{\mathbf{m}} \cdot \hat{\mathbf{n}}, \tag{1.4}$$

where $\hat{\mathbf{m}}$ is a unit vector in the direction of $\mathbf{M}$, $\hat{\mathbf{n}}$ is the normal to the measurement plane, and R_s is the extraordinary Hall coefficient which depends on the electrical resistivity ρ as

$$R_s(\rho) = a\rho + b\rho^2, \tag{1.5}$$

The linear term in Eq. (1.5) is due to a spin-dependent preferred direction in scattering ("skew scattering") [1], which appears when spin-orbit interaction is included in the treatment of scattering from a short-range potential well. The quadratic term is due to a lateral displacement involved in the scattering ("side jump") [2], which becomes evident when scattering of a wave-packet is considered.

Recently, it has been claimed that Berry phase effect [3] in the crystal momentum space ($\mathbf{k}$-space) also gives rise to EHE in some materials [4, 5, 6]. This EHE is intrinsic: it does not involve scattering, but it depends on the occupied Bloch states. In this model, the EHE is described as

$$\rho_{xy}^{EHE} = -\rho^2 \sigma_{xy}^{BP}(M)\, \hat{\mathbf{m}} \cdot \hat{\mathbf{n}}, \tag{1.6}$$

where the Berry phase transverse conductivity $\sigma_{xy}^{BP}(M)$ does not depend on ρ, and the dependence of σ_{xy}^{BP} on M can be calculated from the band structure.[1] In the framework of the semiclassical picture, the equations of motion for an electronic wave

[1] In general, σ_{xy}^{BP} may depend also on the direction of $\mathbf{M}$ relative to the crystal.

packet moving in the n-th band are [7]

$$\dot{\mathbf{r}} = \frac{1}{\hbar}\nabla_{\mathbf{k}}\mathcal{E}_n(\mathbf{k}) - \dot{\mathbf{k}} \times \mathbf{\Omega_n}(\mathbf{k}), \tag{1.7}$$

$$\hbar\dot{\mathbf{k}} = -e(\mathbf{E} + \dot{\mathbf{r}} \times \mathbf{B}), \tag{1.8}$$

where

$$\mathbf{\Omega_n}(\mathbf{k}) = i\nabla_{\mathbf{k}} \times \langle u_n(\mathbf{k})|\nabla_{\mathbf{k}} u_n(\mathbf{k})\rangle \tag{1.9}$$

is the Berry phase curvature, determined by the Bloch functions $e^{i\mathbf{k}\cdot\mathbf{r}}u_n(\mathbf{k})$.[2] While the OHE is described by the second term in Eq. (1.8), the term involving $\mathbf{\Omega_n}(\mathbf{k})$ in Eq. (1.7) does not have a classical counterpart and it represents an additional transverse velocity, which gives rise to the EHE. First, this mechanism was invoked to explain the EHE in (III,Mn)V ferromagnetic semiconductors [4], then in $SrRuO_3$ [5] (which is examined in Chapter 3), and later it was shown that the Berry phase effect in **k**-space should be the dominant mechanism even in iron [6]. Actually the Berry phase mechanism for the EHE has been suggested by Karplus and Luttinger [8, 9][3] fifty years ago, but it has been largely disregarded later.

The **k**-space Berry phase mechanism should be distinguished from the Berry phase effect related to a motion in a topologically non-trivial spin background in *real* space, which recently has been also proposed as a source of EHE for some materials [11].

Finally, Hirsch [12] has analyzed, in the framework of classical electrodynamics,

[2]The Berry phase along a path C in the n-th band is

$$\gamma_n(C) = i\oint_C \langle u_n(\mathbf{k})|\nabla_{\mathbf{k}} u_n(\mathbf{k})\rangle \cdot d\mathbf{k} \tag{1.10}$$

[3]However, the term "Berry phase" does not appear in their work since the Berry phase effect was discovered much later [3]. The relation between this Hall effect and the Berry phase has been noticed by Chang and Niu [10].

the motion of a magnetic moment in a periodic lattice potential. This yields an additional contribution to the EHE with R_s of the order of R_0. Commonly, this contribution does not play an important role because the total R_s is much larger than R_0.

1.2 Strontium ruthenate ($SrRuO_3$)

1.2.1 General

The interest in $SrRuO_3$, a compound which is probably not found in nature, has originally arisen from the possibility of using this material as a metallic electrode or buffer layer in various heterostructure electronic devices which are based on materials with a perovskite-type crystal structure (such materials include high-T_c superconductors and ferroelectrics) [13, 14, 15]. The good thermal conductivity and the remarkable chemical and thermal stability of $SrRuO_3$ (stable up to 1200 K in oxidizing or inert-gas atmospheres [16]; unchanged in structure up to 685 K [17]) are a great advantage for many applications.

In addition to the possible applications, $SrRuO_3$ has drawn much attention in the last few years due to its unusual properties, which in some cases were interesting in themselves, and in other cases provided a convenient playground for investigating general material properties. Some of these properties are described in the foregoing sections.

1.2.2 Crystalline structure

The unit cell of $SrRuO_3$ is shown in Fig. 1.2(a). $SrRuO_3$ belongs to the perovskite group of minerals, which is a group of oxides with a general formula of ABO_3 (in our case A = Sr, B = Ru), which have a common crystalline structure. The BO_3 ions form a framework of corner-sharing octahedra, with a B ion at the center of each octahedron and six O ions at the corners. The A ion is situated between eight such octahedra. In many perovskites the octahedra are tilted or rotated in order to ac-

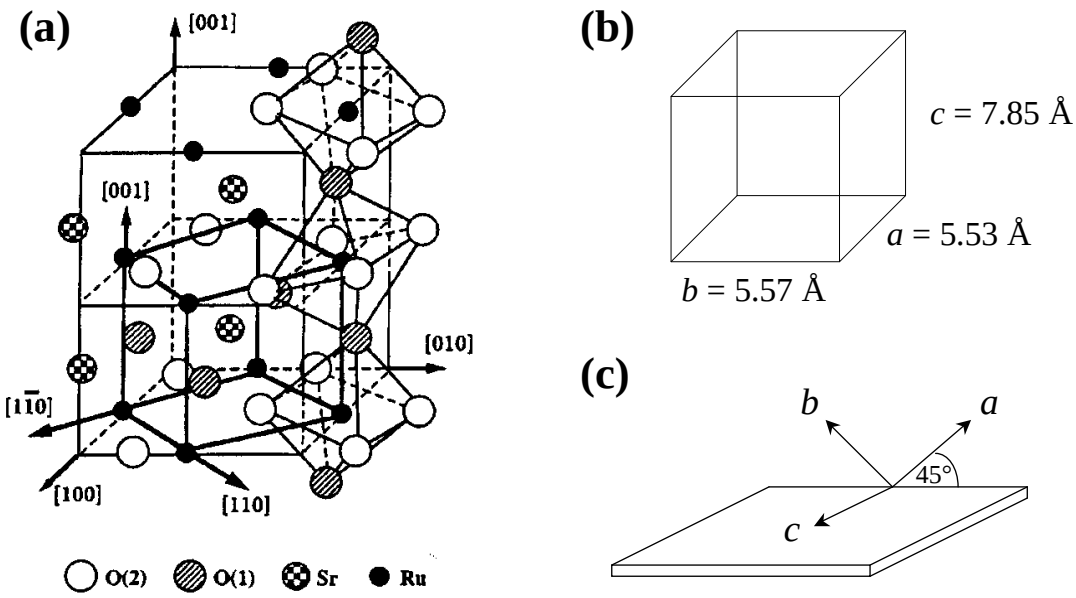

Figure 1.2: Structure of $SrRuO_3$. (a) Unit cell, containing 4 formula units (picture from Ref. [18]). (b) Lattice structure (orthorhombic), where a, b, and c correspond to [100], [010], and [001], respectively. (c) Growth orientation on miscut $SrTiO_3$ substrate.

commodate the large A ions. The result is a variety of symmetries from isometric to tetragonal to orthorhombic to monoclinic depending on the degree of distortion. The unit cells of $SrRuO_3$ (containing 4 formula units) are arranged in an orthorhombic lattice, shown in Fig. 1.2(b). Since the distortion of the octahedra positions in $SrRuO_3$ is not large, its structure can be also described as pseudocubic (the pseudocubic unit cell, with a lattice parameter of 3.93 Å, is also shown in Fig. 1.2(a)).

1.2.3 Electronic properties

$SrRuO_3$ is a metal. However, its electrical resistivity is relatively large ($\rho \sim 200$ $\mu\Omega$ cm at room temperature, even for samples with a residual resistivity of ~ 1 $\mu\Omega$ cm), and it continues to grow with increasing temperature almost without saturation, and

seems to cross the Ioffe-Regel limit [19] (where the mean free path becomes as small as the lattice constants). The exact reason for this behavior is not clear; possibly it is related to strong electronic interactions, which may be implied by the strong T^2 term in the electrical resistivity at low temperatures [20] and the mass enhancement (by a factor of 3.7 relative to band calculations) observed in measurements of the specific heat [19].

Additional abnormal properties of $SrRuO_3$ include: non-Drude behavior of the infrared conductivity [21, 22], violation of the Fisher-Langer relation for the temperature derivative of the resistivity near T_c [20], and deviations from Matthiessen's rule [23, 24] (the latter can be expected in a metal with a short mean free path due to the Pippard ineffectiveness condition [23]).

Despite these irregularities, quantum oscillations in the electrical resistivity of $SrRuO_3$ at high magnetic fields (the Shubnikov–de Haas effect) show the existence of conventional fermion quasiparticles (at least at low temperatures, where the effect is observable) [25].

Band calculations reveal a complicated band structure, and the results of the calculations are sensitive to the input parameters and depend on the method of calculation [19, 26, 27, 28]. A typical result for the density of states is shown in Fig. 1.3. The Fermi surface is dominated by the $4d$ electrons of Ru, which are also primarily responsible for the magnetic moment.

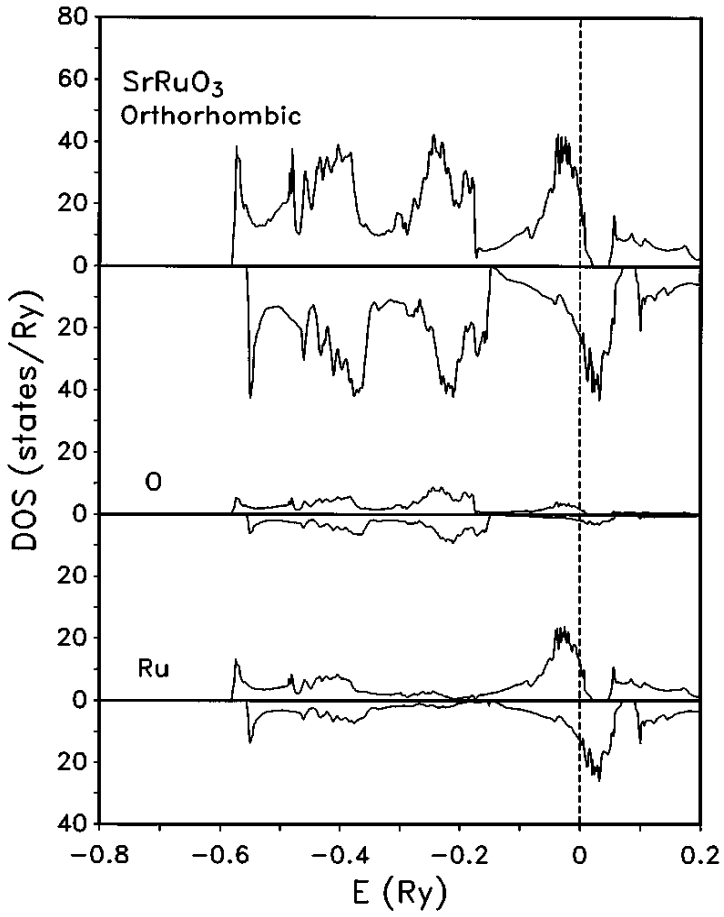

Figure 1.3: Density of states in $SrRuO_3$ (from Ref. [26]). Majority (minority) spin is shown as positive (negative). The partial O (*2p*) and Ru (*4d*) contributions are also shown. The dashed vertical line denotes the Fermi energy.

1.2.4 Magnetic properties

$SrRuO_3$ is a ferromagnet, with a transition temperature T_c of $\sim$ 165 K in crystals, and $\sim$ 150 K in thin films grown on $SrTiO_3$ substrates.[4]

The zero-temperature magnetic moment is about $1.4\mu_B$ per formula unit (or

[4]The films are slightly strained by the substrate due to a small mismatch between the lattice parameters of the (cubic) unit cell of $SrTiO_3$ (3.905 Å) and the pseudocubic unit cell of $SrRuO_3$ (3.93 Å), which is the reason for the different T_c: Gan *et al.* [29] have detached such film from the substrate, and the T_c increased to the bulk-like value.

$M_0 = 210$ emu/cm^3), and originates from the $4d$ electrons of the Ru atoms (see Fig. 1.3). These are also the conduction electrons, so that $SrRuO_3$ is an itinerant ferromagnet. Consequently, significant spin polarization of the conduction electrons exists in $SrRuO_3$ [30].

The temperature dependence of the ferromagnetism of $SrRuO_3$ should be probably described in terms of the local-band model [31], since there is evidence from spectroscopic measurements that the ferromagnetic band splitting in $SrRuO_3$, as in many other itinerant ferromagnets, does not disappear at T_c [32]. This means that as the temperature is increased to T_c, the magnetization disappears only on the long scale, but short-range order remains; the band splitting will disappear only at some temperature $T_S \gg T_c$.

In the ferromagnetic state, $SrRuO_3$ films grown on miscut $SrTiO_3$ substrates possess a single easy axis of magnetization, roughly in the b orthorhombic direction [33, 34]. At T_c, the easy axis points strictly along the b direction (45° out of the film plane), and it slowly rotates as a function of temperature at a rate of 0.1°/K toward the normal to the film (up to 30° relative to the normal at $T = 0$) [34].

The magnetic anisotropy in $SrRuO_3$ films is relatively large: the anisotropy constants are of the order of $K \sim 10^7$ erg/cm^3 [35, 36], corresponding to an effective anisotropy field of about 10 T. The large anisotropy constant (compared to 5×10^5 erg/cm^3 in iron [37], 8×10^5 erg/cm^3 in nickel [38], and 4×10^6 erg/cm^3 in hcp cobalt [39]) is probably a result of the reduced symmetry[5] (see Fig. 1.2) and the large spin-

[5] A remarkable example of the dependence of the magnetic anisotropy on the crystal symmetry is the order-of-magnitude difference in the anisotropy constants between hcp and fcc cobalt [39].

orbit coupling,[6] through which the spin direction is affected by the crystal structure. Shape anisotropy is negligible, since $2\pi M_0^2 \sim 3 \times 10^5$ erg/cm$^3 \ll K$.

1.2.5 Magnetotransport properties

Throughout most of the temperature range (from $T \sim 10$ K up to at least room temperature) the electrical resistivity of $SrRuO_3$ decreases when a magnetic field **H** is applied, i.e., the magnetoresistance (MR) $\Delta\rho(H) \equiv \rho(H) - \rho(0)$ is negative. The strongest MR ($\Delta\rho/\rho \sim 10\%$ for $H \sim 10$ T) is observed near T_c. This indicates that the MR is related mostly to diminishing of spin-dependent scattering (since the field-induced enhancement of magnetization is most significant near T_c). A comprehensive analysis of the relation of the MR to changes in magnetization is presented in Appendix A.

The MR in $SrRuO_3$ is anisotropic; it depends on the directions of both the current and the magnetization relative to the crystalline directions [41].

At low temperatures (below about 10 K) the MR becomes positive [42]. This is expected due to shortening of the mean free path due to the Lorentz force. The positive MR is most significant in samples with low residual resistivity, and it becomes stronger as the temperature is lowered. These observations are in agreement with the expectation that the Lorentz MR is most significant when the mean free path is long.

[6] The spin-orbit coupling constant ζ in Ru ion (~ 900 cm^{-1}) is significantly larger than, for example, in Fe (~ 400 cm^{-1}), Ni (~ 600 cm^{-1}), and Co (~ 500 cm^{-1}) [40].

1.3 EHE in $SrRuO_3$

It has been found [43, 44] that the EHE due to the spontaneous magnetization in the ferromagnetic phase of $SrRuO_3$ exhibits a non-monotonic temperature dependence, including a change of sign at $T \simeq 130$ K, as shown in Fig. 1.4. The behavior

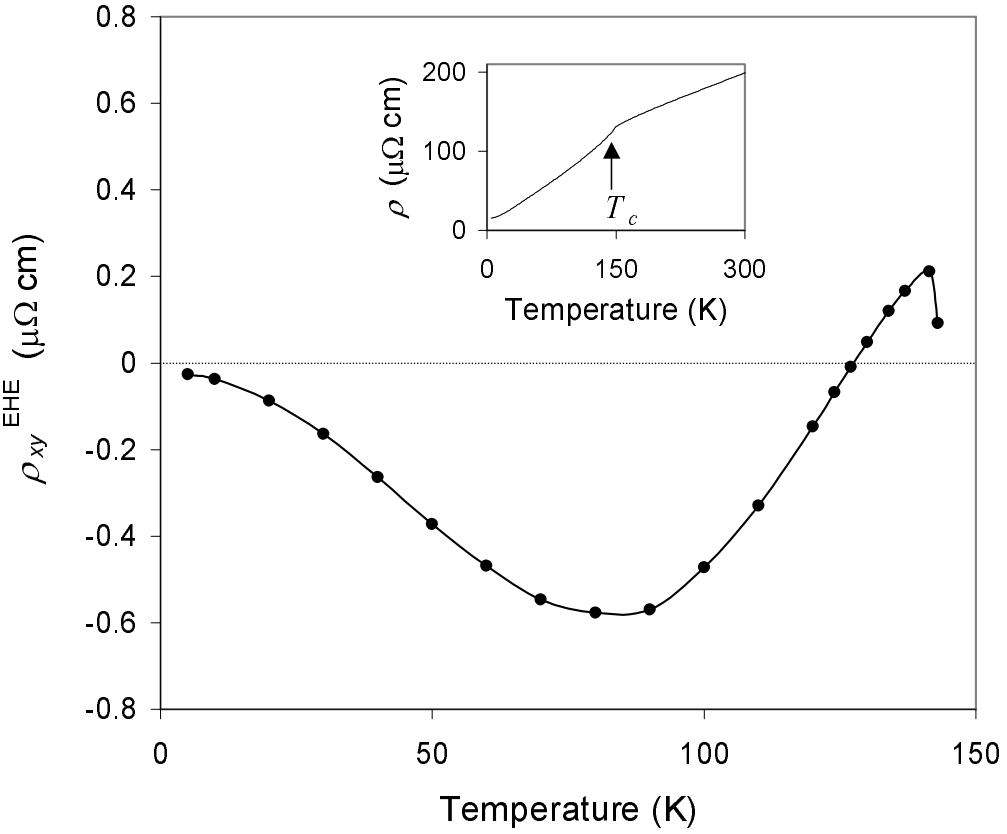

Figure 1.4: Extraordinary Hall effect ρ_{xy}^{EHE} (due to the spontaneous magnetization) as a function of temperature. The inset shows the longitudinal resistivity ρ as a function of temperature.

of the EHE coefficient R_s as a function of resistivity cannot be fitted with Eq. (1.5), as is evident from Fig. 1.5. This is one of the reasons for the interest in the EHE in this compound.

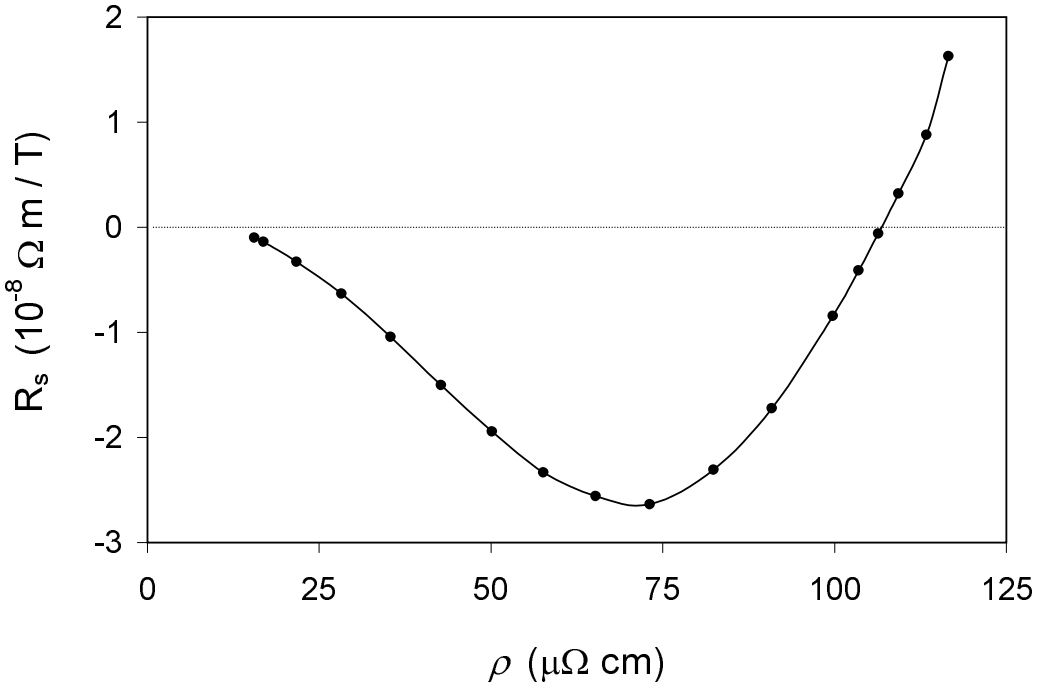

Figure 1.5: EHE coefficient R_s (at the spontaneous magnetization) as a function of the temperature-dependent resistivity ρ. (The connecting line is a guide to the eye.)

In the current work we perform measurements of the EHE as a function of the magnetic field. Since the correlation between changes in M and ρ is different in temperature-dependent measurements and field-dependent measurements, the latter provide a new degree of freedom for testing the dependence of the EHE on M and ρ. This method allows us to reach several definite conclusions as to the mechanism behind the EHE in $SrRuO_3$. These results are described in Chapter 3. We also extend the EHE measurements to the paramagnetic phase, as described in Chapter 4. And in Chapter 5 we test the dependence of the EHE on the direction of the magnetization, and observe a non-trivial behavior.

Chapter 2

Experimental Details

2.1 Samples of $SrRuO_3$

2.1.1 Thin film growth

Because of its complicated composition, the growth of $SrRuO_3$ as either bulk crystals or thin films is not trivial. Epitaxial growth of films on various substrates and under various conditions has been attempted [14, 45, 46].

In general, even when an exact stoicheometry is achieved, a mixture of several growth orientations of the pseudocubic $SrRuO_3$ on a cubic or pseudocubic substrate can appear (see, e.g., Ref. [33] about $SrRuO_3$ on $SrTiO_3$ substrates). Mixed-orientation samples are of limited usefulness for research purposes, since the measured quantities are averaged over the different orientations. Furthermore, it can be problematic to magnetize such samples, since the easy axis points at different directions for grains with different orientations. For the same reason, it is not possible to

perform measurements in a magnetic field without involving changes in the direction of the intrinsic magnetization.

It was found [14, 45] that it is possible to grow single-orientation films of $SrRuO_3$ on the (001) face of a (cubic) $SrTiO_3$ crystal, if it is miscut by $\sim 2^\circ$ toward [010]. Such films grow with the orthorhombic [110] direction perpendicular to the surface (as was shown by x-ray diffraction [14] and by electron diffraction combined with Lorentz imaging [33]), so that the a and b directions are at 45° out of the plane of the film (see Fig. 1.2(c)).

Single-orientation thin films of $SrRuO_3$ grown on miscut $SrTiO_3$ substrates were available to us through a collaboration with the Kapitulnik-Geballe-Beasley (KGB) group at Stanford University. The films were grown by reactive electron beam evaporation [47], by James W. Reiner [35] while being a Ph. D. student of M. R. Beasley.

2.1.2 Sample preparation

We patterned the films by photolithography to allow precise measurement of longitudinal and Hall resistance (a typical pattern scheme is shown in Fig. 2.1). Aluminum wires were attached to the contact pads by a wire bonder.

2.1.3 Sample characterization

We ensured that the measured samples were not composed of grains with different crystallographic orientations by measuring resistivity below T_c while the samples are rotated relative to an applied magnetic field $\mathbf{H}$. Jumps in resistivity (due to mag-

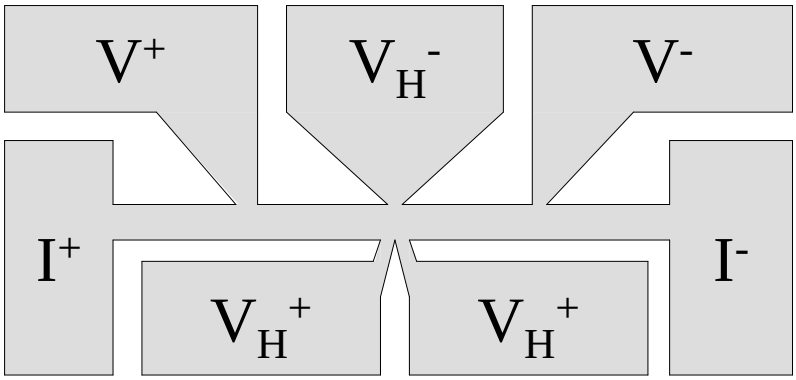

Figure 2.1: A typical pattern for measurement of resistivity and Hall effect. The current wires are connected to pads I^+ and I^-, the longitudinal voltage is measured between pads V^+ and V^-, and the Hall voltage is measured between pads V_H^+ (any of them) and V_H^-. The width of the current path is 50 μm.

netization reversal) occur when **H** is perpendicular to the easy axis,[1,2] as shown in Fig. 2.2 for a single-orientation sample at $T = 40$ K. The jumps in Fig. 2.2 occur at $\theta \simeq 120^\circ$ and $\theta \simeq -60^\circ$, indicating that the easy axis is at $\theta \simeq -30^\circ$, in agreement with direct measurements of magnetization on similar films, mentioned in Sec. 1.2.4. In samples which involve a mixture of several orientations, jumps occur at additional angles, corresponding to configurations with different orientations of the easy axis. Samples grown on miscut $SrTiO_3$ substrates usually included a single orientation, while samples grown on strictly (001) $SrTiO_3$ substrates usually included grains with various orientations.

One measure for a quality of a film is its residual resistivity ρ_0 (i.e., the resistivity

[1]More generally: perpendicular to the projection of easy axis on the rotation plane.

[2]As the field is rotated away from the easy axis, the magnetization also deviates from the easy axis, but it does not follow the field because of the large magnetic anisotropy. As a result, when the field is perpendicular to the easy axis, the magnetization abruptly changes its orientation between two non-collinear directions. Due to the anisotropic magnetoresistance (see Sec. 1.2.5) the resistivity is different before and after this magnetization switching.

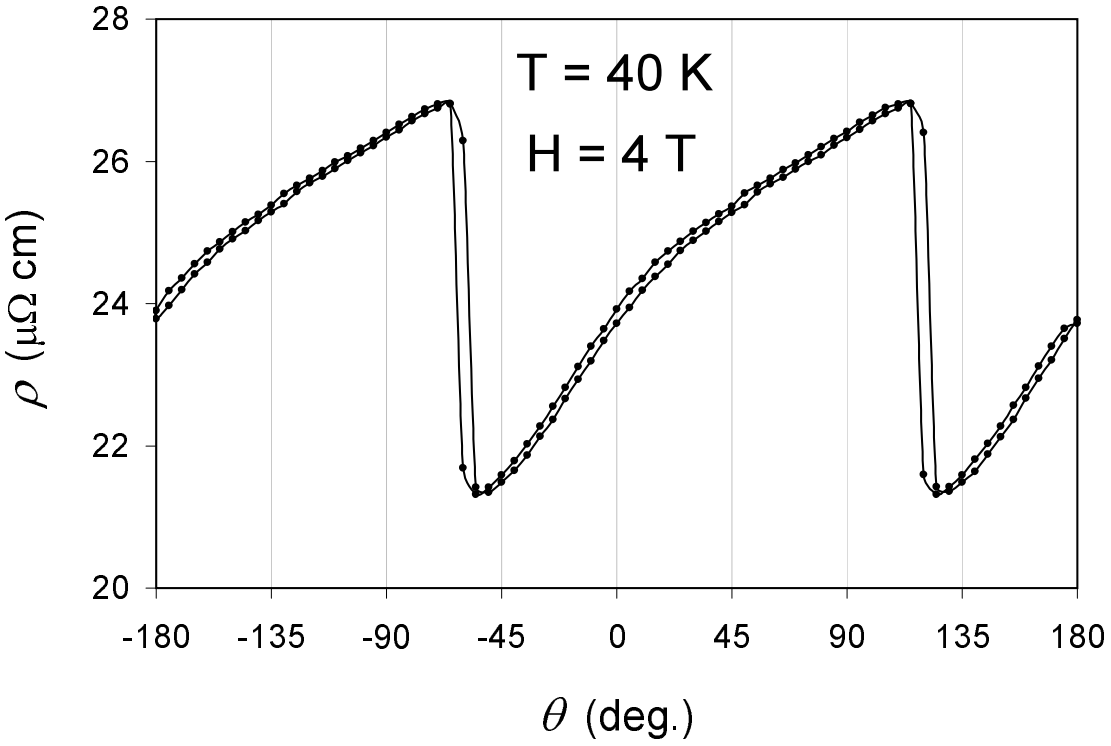

Figure 2.2: Resistivity of a single-orientation film as a function of the magnetic field direction (θ is measured relative to the normal to the film, in the (001) plane) at $T = 40$ K, $H = 4$ T. (The two curves correspond to sweeps forwards and backwards in the angle.)

ρ in the limit $T \to 0$), since the residual resistivity in metals is caused by crystal defects and impurities. Therefore, among the samples available to us, the ones which had lower residual resistivities ($\rho_0 \sim 5 - 10$ $\mu\Omega$ cm, while the room temperature resistivity is about 200 $\mu\Omega$ cm) were used.

We have studied films of various thicknesses (10−200 nm), and obtained essentially thickness-independent results, except for a decrease in T_c with decreasing thickness (from $T_c \sim 153$ K in the thick film limit down to $T_c \sim 145$ K in a 10-nm film) and the corresponding rescaling of the temperature dependence of the related quantities close to T_c.

2.2 Measurement system

Low-temperature, high-magnetic-field measurements were performed in the Quantum Design Physical Property Measurement System (PPMS). This system includes a liquid helium cryostat with a superconducting magnet.

The system allows us to make measurements between 1.8 and 400 K, with a temperature stability of about 0.01% after a half-hour stabilization. Effects of short-time fluctuations in temperature can be avoided by averaging the measured quantity over time (5-15 minutes) at each measurement point.[3] In some of our experiments (particularly, in the extraction of the OHE described in Sec. 2.3.3) a better temperature stabilization was required. It was achieved by a longer stabilization time (> 10 hours). Magnetic fields up to 9 T are available, with a reproducibility of about ± 1 mT.

The sample can be mounted on a rotator, which allows it to be positioned at various angles relative to the magnetic field, with an accuracy of $\sim 2^\circ$ and a reproducibility of $\sim 1^\circ$.

[3] This method of averaging is limited, however, by the non-linearity in the temperature dependence of the measured quantity, if measurements with a high resolution in temperature are required.

2.3 Special considerations

2.3.1 Magnetizing the sample

It is common in ferromagnets that in order to reduce magnetostatic energy the sample subdivides into domains with different directions of the magnetization. When a magnetic field is applied, domains with magnetization parallel to the field grow, while the opposite domains shrink and eventually disappear. However, when the field is turned off, the domains reappear. As a result, magnetic measurements at low fields are affected not only by field-induced changes of the intrinsic magnetization, but also by the rearrangement of the domains. In many cases, this hinders the possibility of field-dependent measurements of the intrinsic behavior.

In $SrRuO_3$ the situation is different. Due to the large anisotropy ($H_{anis} \sim 10$ T) and the small self field ($4\pi M \sim 0.2$ T), once the sample is magnetized by applying a sufficiently high magnetic field (several teslas) it remains uniformly magnetized (does not subdivide into domains) even at zero field. The domains renucleate only when a sufficient field in the opposite direction is applied (except a few degrees below T_c where the domains renucleate at a low positive field) [33]. This property allows us to perform field-dependent measurements down to zero field. Furthermore, since the field at which magnetization reversal starts is observed in sweeps of resistivity or Hall effect versus field, we were able to ensure this property for every sample and at every temperature. All measurements reported in this work were performed with the sample uniformly magnetized.

2.3.2 Cancellation of longitudinal offset in Hall measurements

In measurements of the Hall effect, some misalignment of the Hall voltage contacts usually exists between the two sides of the current path. As a result, the measured voltage $\widetilde{V}_H$ includes some contribution of a longitudinal voltage (which is also commonly field-dependent and magnetization-dependent). However, since the longitudinal contribution remains the same when the directions of **B** and **M** are reversed, the Hall voltage can be determined as:

$$V_H(\mathbf{B},\mathbf{M}) = \frac{\widetilde{V}_H(\mathbf{B},\mathbf{M}) - \widetilde{V}_H(-\mathbf{B},-\mathbf{M})}{2}. \tag{2.1}$$

A configuration with reversed directions of **B** and **M** is achieved by reversing the direction of the applied magnetic field $\mathbf{H}_{ext}$ (in the measurement itself and in the preliminary procedures, such as magnetizing the sample in a specific direction).

2.3.3 Identification of the ordinary Hall effect

A crucial issue in an experimental investigation of the EHE is the separation between the EHE and the OHE, since both of them change as a function of the magnetic field. In the ferromagnetic phase, the changes in M are usually much smaller than the applied fields: $\Delta M \ll B$. However, usually $R_s \gg R_0$. Therefore, neither of these effects can be neglected. For the same reason, neither can any of them be neglected in the paramagnetic phase, even though the induced magnetization is small ($M \ll B$).

This issue becomes particularly important when models such as suggested by Fang *et al.* [5] are considered (to be discussed in Chapter 3), since they predict a high sensitivity of the EHE to the value of M, therefore it is not straightforward how to

measure the OHE separately. In the conventional models, the possible ρ-dependence of R_s should be taken into account, since a magnetic field can induce changes in ρ.

We found a way to separate between the OHE and the EHE without making assumptions about the model behind the EHE, or the reason due to which the EHE changes as a function of field. We measured the Hall effect at a low magnetic field ($H \sim 0.4$ T) as a function of the direction of the field. In such fields, the change in ρ_{xy} is linear in H, implying that the change in ρ_{xy}^{EHE} is also linear in H.[4] In addition, for such fields $\mathbf{M}$ does not rotate away from the easy axis (because the anisotropy field is of order of 10 T).[5] Since the easy axis is at $\alpha \simeq 45^\circ$ (see Fig. 2.3), the EHE and the OHE contributions have different symmetries, and can be separated. Particularly, the EHE contribution should not be affected at all when the magnetic field is applied perpendicularly to the easy axis.

Figure 2.4 shows the additional Hall effect (i.e., after subtracting the EHE measured at zero field) as a function of the direction of the field. The additional Hall effect does not vanish when the magnetic field is in-plane ($\alpha = 90^\circ$), indicating that not only the OHE is involved. Neither does it vanish when the magnetic field is perpendicular to the easy axis ($\alpha = 133^\circ$), indicating that not only the EHE plays a role.

[4] This implication is correct if the change in ρ_{xy}^{EHE} is not much smaller than the total change in ρ_{xy}, which turns out to be correct in our case.

[5] For example, when a field of 0.4 T is applied at 60° relative to the easy axis, the magnetization rotates by about 1°. If the possible dependence of the EHE on the direction of $\mathbf{M}$ due to material anisotropy is neglected (and only the trivial geometric dependence is taken into account), the error due to incorrect modeling of the *field-induced* change in the Hall effect is only about 4% of it. The additional error due to change in the *zero-field* EHE can be made smaller than that error if the measurement is performed at a temperature where the zero-field EHE is small, as we did ($T = 127$ K).

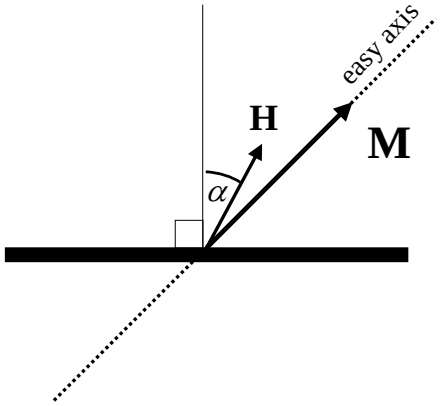

Figure 2.3: Experiment for separating the EHE and the OHE.

The behavior can be fitted as a sum of the OHE and the EHE contributions according to the formula

$$\Delta\rho_{xy} = R_0 H\cos\alpha + \frac{d\rho_{xy}^{EHE}}{dM}\chi H\cos(\alpha-\alpha_{ea}), \tag{2.2}$$

or

$$\frac{\Delta\rho_{xy}}{H} = \left(R_0 + \frac{d\rho_{xy}^{EHE}}{dM}\chi\cos\alpha_{ea}\right)\cos\alpha + \left(\frac{d\rho_{xy}^{EHE}}{dM}\chi\sin\alpha_{ea}\right)\sin\alpha, \tag{2.3}$$

where α_{ea} is the direction of the easy axis, and χ is the magnetic susceptibility.

The fit is shown in Fig. 2.4. It turns out that the parts of the OHE and the EHE in the field-induced Hall effect were comparable in magnitude. For a field applied along the easy axis: $(60\pm3)\%$ of the change in Hall effect was due to the OHE, while $(40\pm3)\%$ was due to the EHE.

The OHE coefficient is $R_0 = (-4\pm1)\times10^{-10}$ Ω m/T, where nearly half of the error is due to uncertainties in fitting, and the other half is due to uncertainty (of about 15%) in film thickness.[6] This corresponds to an electronic charge density of

[6]However, the error due to uncertainty in film thickness does not play a role when we use the

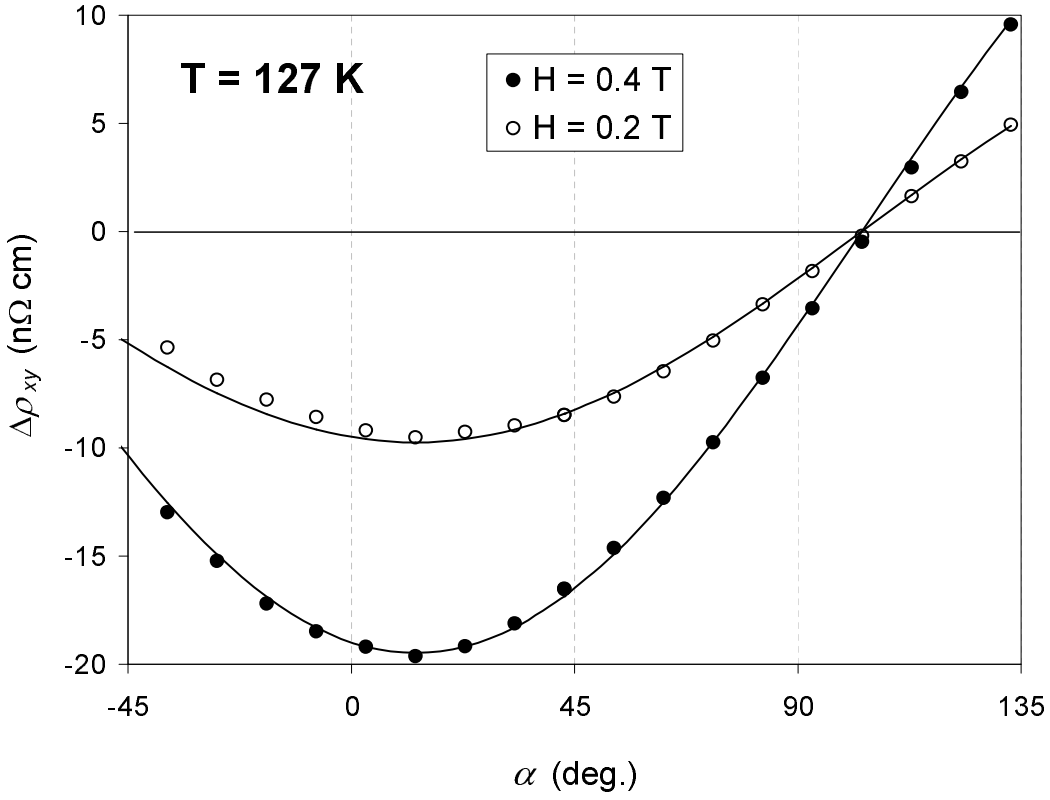

Figure 2.4: Field-induced contribution to the Hall effect as a function of the direction of the field (the angle α is defined in Fig. 2.3). The solid curves are fits from which the OHE and the EHE contributions were evaluated.

$n = (1.6 \pm 0.4) \times 10^{22}$ cm^{-3}, which is 1.0 electron per formula unit.

value of R_0 to separate between the OHE and the EHE in the same sample (at different temperatures and fields), since the OHE and the EHE have the same dependence on the thickness.

Chapter 3

Testing the Berry Phase Model for EHE

3.1 Introduction

Fang *et al.* [5] have argued that the strange behavior of the EHE in $SrRuO_3$ (as presented in Sec. 1.3) can be explained in terms of the Berry phase effect in **k**-space (see Eq. (1.6)), which predicts a peculiar non-monotonic dependence of σ_{xy}^{BP} on M. The authors supported their contention by band calculations, which predicted EHE of a correct order of magnitude and roughly reproduced its temperature dependence. However, band calculations for $SrRuO_3$ are very sensitive to the input parameters [5, 28]. Therefore, while the calculations support the explanation, they leave open the possibility that in practice the Berry phase effect in $SrRuO_3$ is much smaller, and the EHE is caused by a different mechanism.

Another point which raises questions regarding the applicability of the calculations of Fang *et al.* is their assumption that the exchange band splitting vanishes at T_c, which is probably not correct for $SrRuO_3$, as described in Sec. 1.2.4. According to the calculation of Fang *et al.*, the EHE changes sign when the band splitting is about 1/3 of its zero-temperature value, which probably does not happen below T_c.

The experiment described in this Chapter is designed to test the applicability of the model suggested by Fang *et al.* by a different kind of measurement.

3.2 Experiment

While in previous experiments the EHE was varied by changing temperature, the experiment presented here explores changes in the EHE resulting from changes in M due to a magnetic field applied at a fixed temperature. This allows us to test the applicability of the Berry phase model directly, by a comparison between temperature-dependent and field-dependent behavior, without making assumptions regarding the details of the band structure. Particularly, we can inquire whether the quantity which vanishes at $T \simeq 127$ K in Fig. 1.4 is the M-dependent σ_{xy}^{BP} of the Berry phase model [Eq. (1.6)] or the ρ-dependent R_s of the extrinsic models [Eq. (1.4)].

In our experiment, the magnetic field was applied along the easy axis, in order to create maximal possible changes in M. All measurements were performed with the

films uniformly magnetized, including at zero magnetic field (see Sec. 2.3.1). The film whose results are presented here has a thickness of 30 nm, and $T_c \simeq 147$ K.

3.3 Results and analysis

Figure 3.1 presents the Hall effect as a function of the magnetic field H at different temperatures. It includes both OHE and EHE. Figure 3.2 shows the EHE, after the OHE was subtracted based on the value determined in Sec. 2.3.3. Interestingly, while the magnetization increases with increasing field, not only does the EHE decrease, it even changes sign. Furthermore, EHE exists even at $T = 127$ K, where the zero-field R_s (as implied from Fig. 1.4) vanishes.

These results seem to qualitatively agree with the predictions of the Berry phase model for these temperatures, since by applying a magnetic field we reach values of M which at zero field exist at lower temperatures: Figure 1.4 implies that in the range of temperatures presented in Fig. 3.2, $|\sigma_{xy}^{BP}(M)|$ decreases with increasing M; therefore, the EHE is expected to decrease when magnetic field is applied.

On the other hand, the increase in M diminishes magnetic scattering, resulting in a negative magnetoresistance (MR) $\Delta\rho(H) = \rho(H) - \rho(0)$ (see Fig. 3.3). Thus the results can qualitatively agree also with the prediction based on Eq. (1.4), since by applying a magnetic field we attain lower resistivities ρ, and in our range of

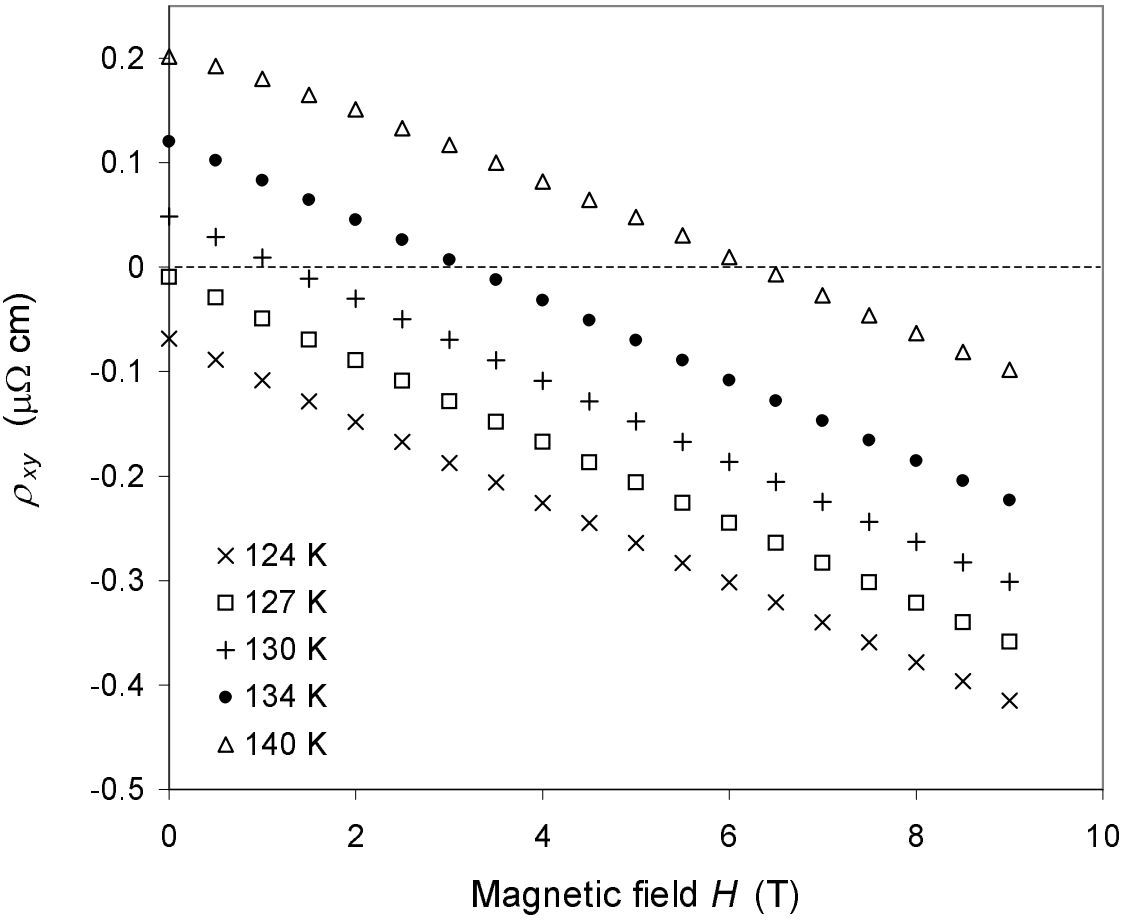

Figure 3.1: Total Hall effect as a function of the magnetic field H at several temperatures (indicated in the legend).

temperatures R_s decreases with decreasing resistivity (see Figs. 1.4 and 1.5).

Quantitative examination of the results supports the second possibility. It turns out, for example, that the MR ($\simeq -7$ $\mu\Omega$ cm) which is required at $T = 134$ K to make the EHE vanish brings the resistivity to the zero-field resistivity of $T = 127$ K (where the EHE vanishes at zero field). Figure 3.4 shows this pattern for a range of temperatures: the EHE always vanishes at the same value of ρ. This behavior is consistent with the extrinsic models [Eq. (1.4)].

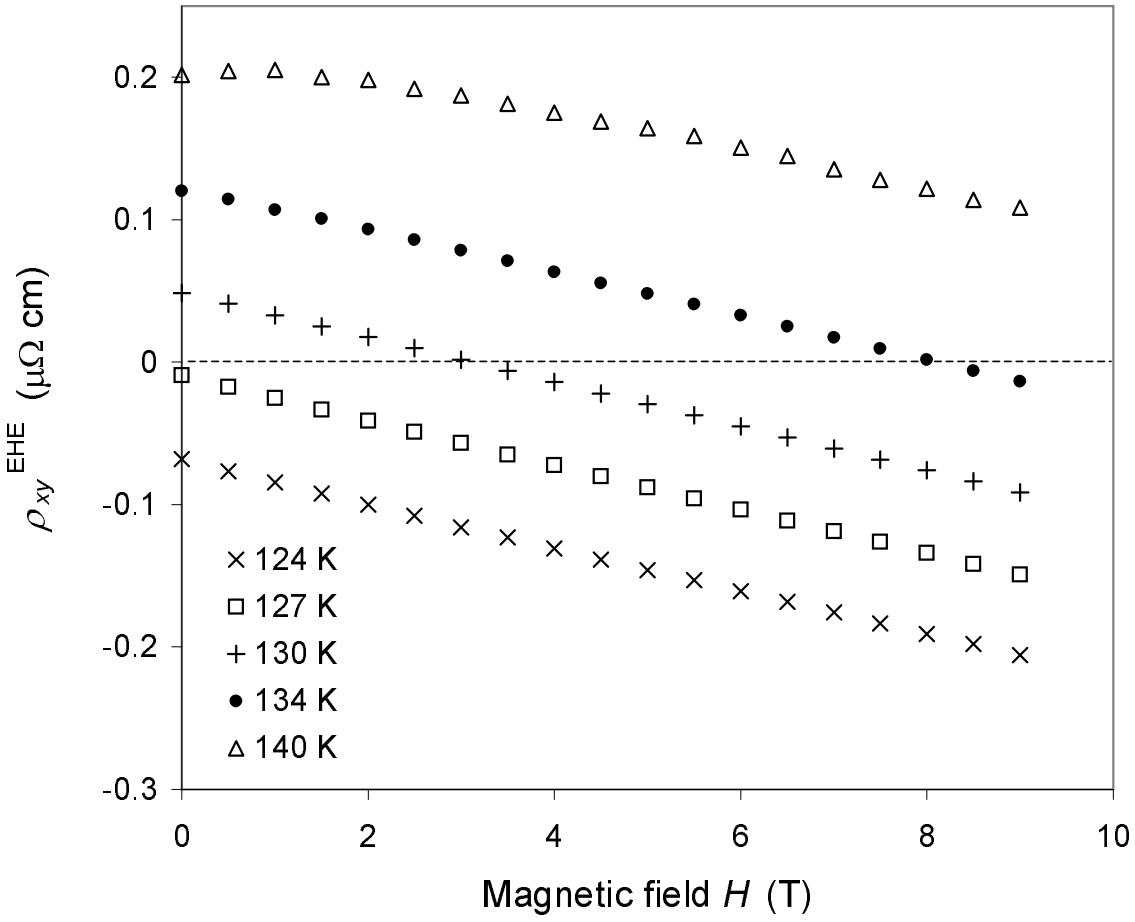

Figure 3.2: Extraordinary Hall effect as a function of the magnetic field H at several temperatures (indicated in the legend).

The vanishing of EHE at constant resistivity cannot be consistent with the Berry phase model [Eq. (1.6)] as well, since the identical resistivities do not correspond to identical values of M, as can be understood by considering changes in magnetic scattering involved in our experiment.

From a temperature $T > 127$ K, vanishing EHE can be achieved either by lowering the temperature to 127 K or by applying an appropriate magnetic field. In both cases ρ decreases to the same value. However, in the first case the decrease in ρ is partly

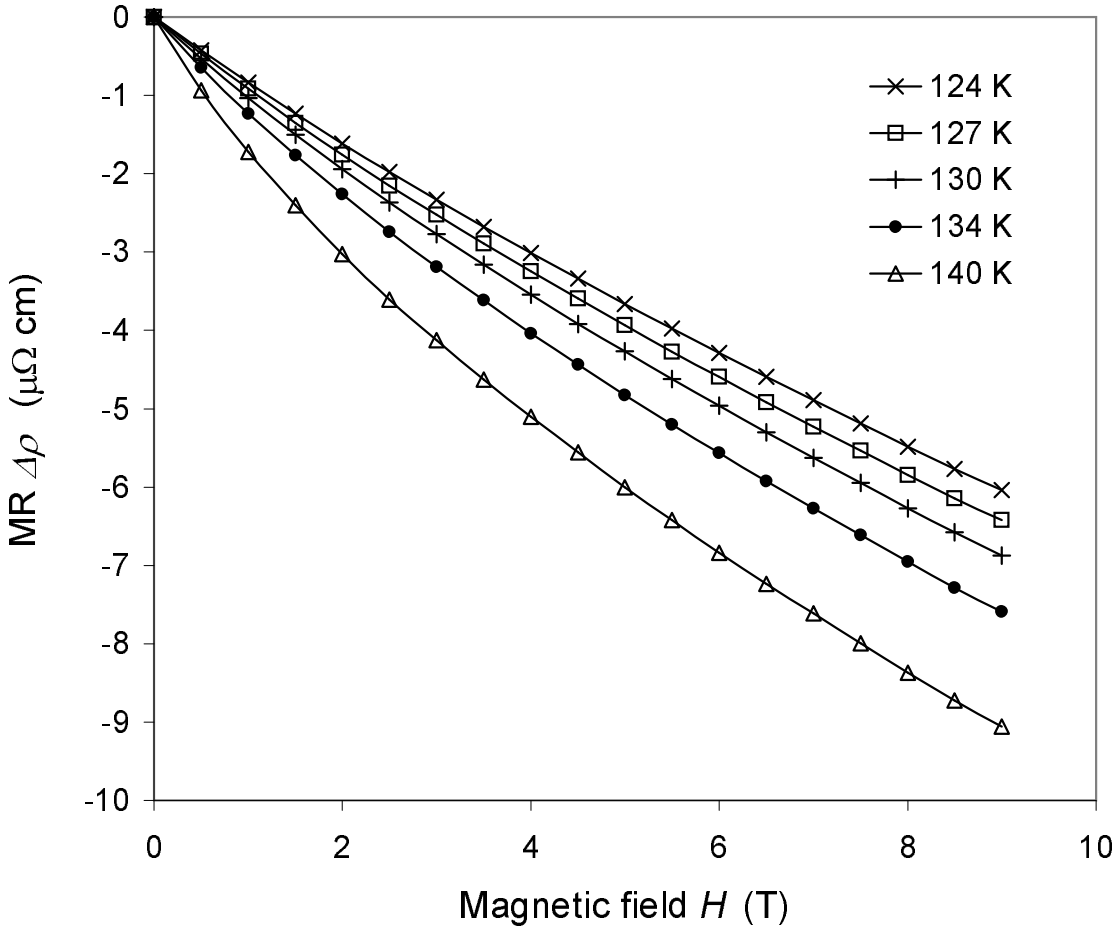

Figure 3.3: Magnetoresistance $\Delta\rho(H) = \rho(H) - \rho(0)$ as a function of the magnetic field H, corresponding to the measurements presented in Fig. 3.2.

related to a decrease in non-magnetic scattering (phonons, etc.), while in the second case the whole change in ρ is due to change in magnetic scattering (see Sec. 1.2.5 and Appendix A). Therefore, the magnetic scattering is different in the two cases, indicating different values of M. Thus, it is not a particular value of M in $\sigma_{xy}^{BP}(M)$ which makes EHE vanish.

Quantitatively, we estimate that the non-magnetic part of $d\rho/dT$ around 130 K is about 0.50 $\mu\Omega$ cm/K, which is the value of $d\rho/dT$ above T_c where the magnetic

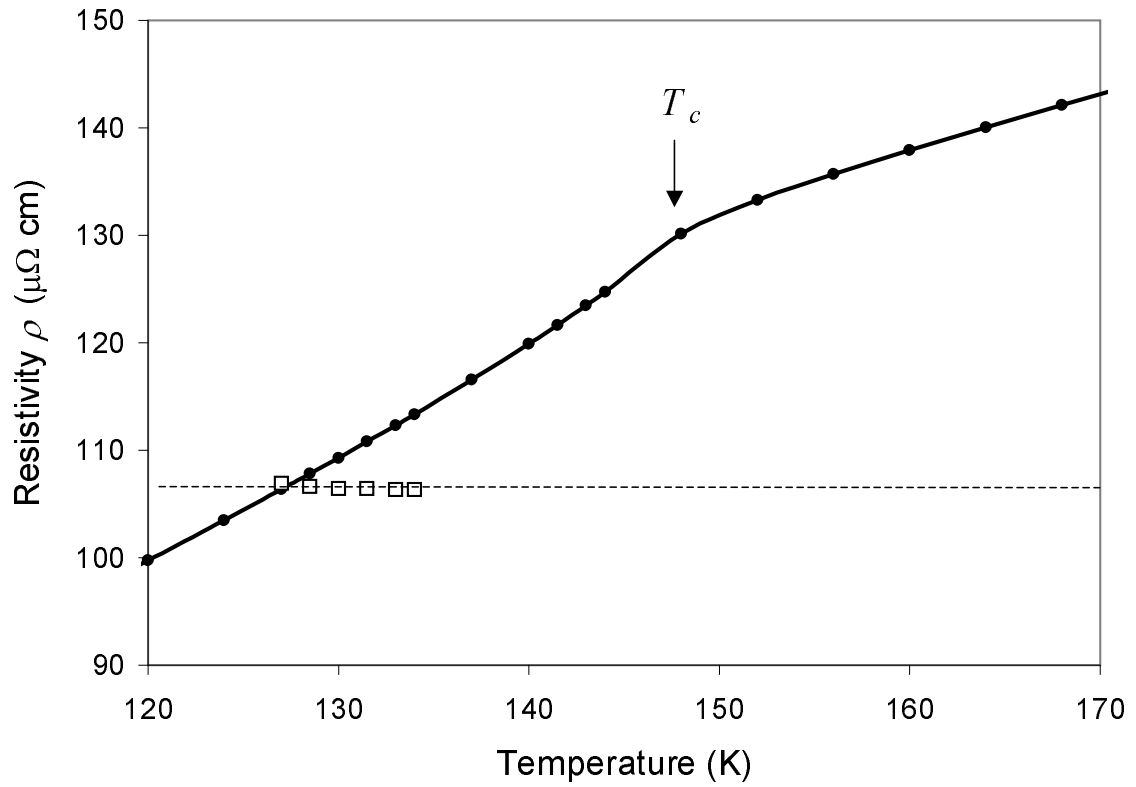

Figure 3.4: The solid curve shows the temperature dependence of the zero-field resistivity ρ, and the squares denote the resistivity for which EHE vanishes at applied magnetic field, as a function of the temperature at which the field is applied.

resistivity saturates. Therefore, non-magnetic resistivity which plays a role in our argument is not negligible. For example, only 3.5 $\mu\Omega$ cm of the 7 $\mu\Omega$ cm difference in the zero-field resistivity between 134 and 127 K is due to magnetic resistivity. The magnetic resistivity of 127 K is achieved at 134 K already for $H = 3.4$ T (this is the field for which the MR is 3.5 $\mu\Omega$ cm, see Fig. 3.3), while the EHE vanishes only at $H = 8.1$ T.

3.4 Conclusions

The Berry phase model for the EHE in $SrRuO_3$ turns out to be inconsistent when temperature-dependent and field-dependent measurements are compared. On the other hand, it seems that Eq. (1.4) describes the EHE correctly, although the microscopic origin of the ρ-dependence of R_s remains unclear.

Chapter 4

EHE in the Paramagnetic State. Anisotropy of the Paramagnetic Susceptibility

4.1 Introduction

As mentioned in Sec. 1.3, the microscopic origin of the ρ-dependence of R_s in $SrRuO_3$ is unclear, since it is not fitted by the conventional expression, Eq. (1.5). Therefore, it may be useful to extend the range of ρ for which R_s is known. Since ρ grows as a function of temperature, it could be useful to extend the measurements of the EHE to $T > T_c$. The magnetization there can be created by applying a magnetic field.

In measurements above T_c we found that a significant Hall effect develops even when the magnetic field **H** is applied parallel to the current which flows along the $[1\bar{1}0]$

direction. The temperature dependence of this Hall effect (see Fig. 4.1) resembles the expected behavior of the induced magnetization. These results indicate that the

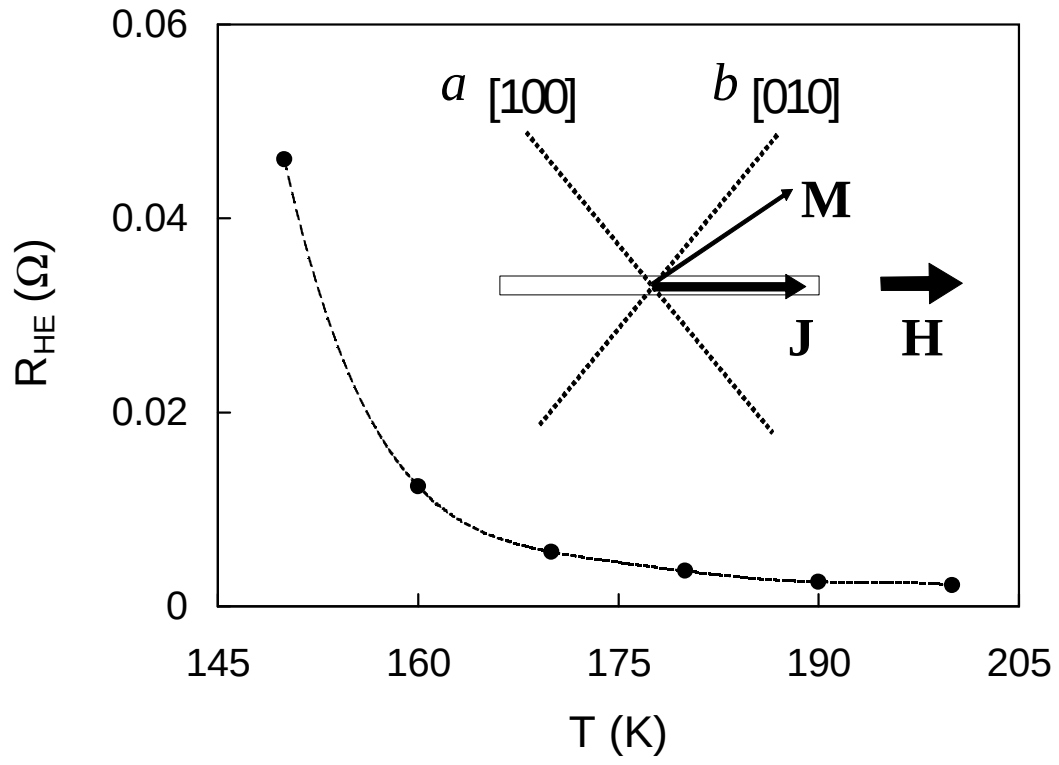

Figure 4.1: Hall effect with $H = 250$ Oe applied parallel to the current (along the $[1\bar{1}0]$ direction) as a function of temperature above T_c ($\simeq 147$ K). The dashed line is a guide to the eye.

in-plane field **H** creates a magnetization **M** possessing an out-of-plane component, which creates a measurable EHE. This shows that the paramagnetic susceptibility is anisotropic, and reveals the EHE as a tool which can be used to investigate the magnetic properties of $SrRuO_3$ in the paramagnetic state. We took advantage of this opportunity, so that the experiment described below, in addition to providing information about the EHE, reveals an interesting behavior of the paramagnetic susceptibility in $SrRuO_3$.

4.2 Experiment

We measured the Hall effect of $SrRuO_3$ films from T_c ($\sim$ 150 K) up to 300 K, as a function of the magnitude and direction of the applied magnetic field. We studied films with thicknesses from 6 to 150 nm, and obtained almost thickness-independent results. The Hall effect data presented below are from a 30-nm film. The OHE was subtracted based on the value determined in Sec. 2.3.3, assuming it to be temperature-independent.[1]

4.3 Results

For quantitative characterization of the susceptibility anisotropy, we measured the Hall effect as a function of field direction at various temperatures. For each temperature above T_c, a small-field limit exists, where the magnetization depends linearly on the field and can be fully described in terms of constant susceptibilities χ_a, χ_b, and χ_c along the a, b, and c crystallographic directions, respectively ($\mu_0 M_a = \chi_a H_a$, etc). An example of measurements in this limit is shown in Fig. 4.2, where the EHE resistance ($R_{EHE} = \mu_0 R_s M_\perp / t$, where t is the thickness of the sample) is shown for two different fields at $T = 153$ K as a function of the angle θ (see inset). The solid curve is a fit obtained by assuming certain values of χ_a and χ_b, based on

[1] The possible errors due to this assumption are analyzed in the discussion.

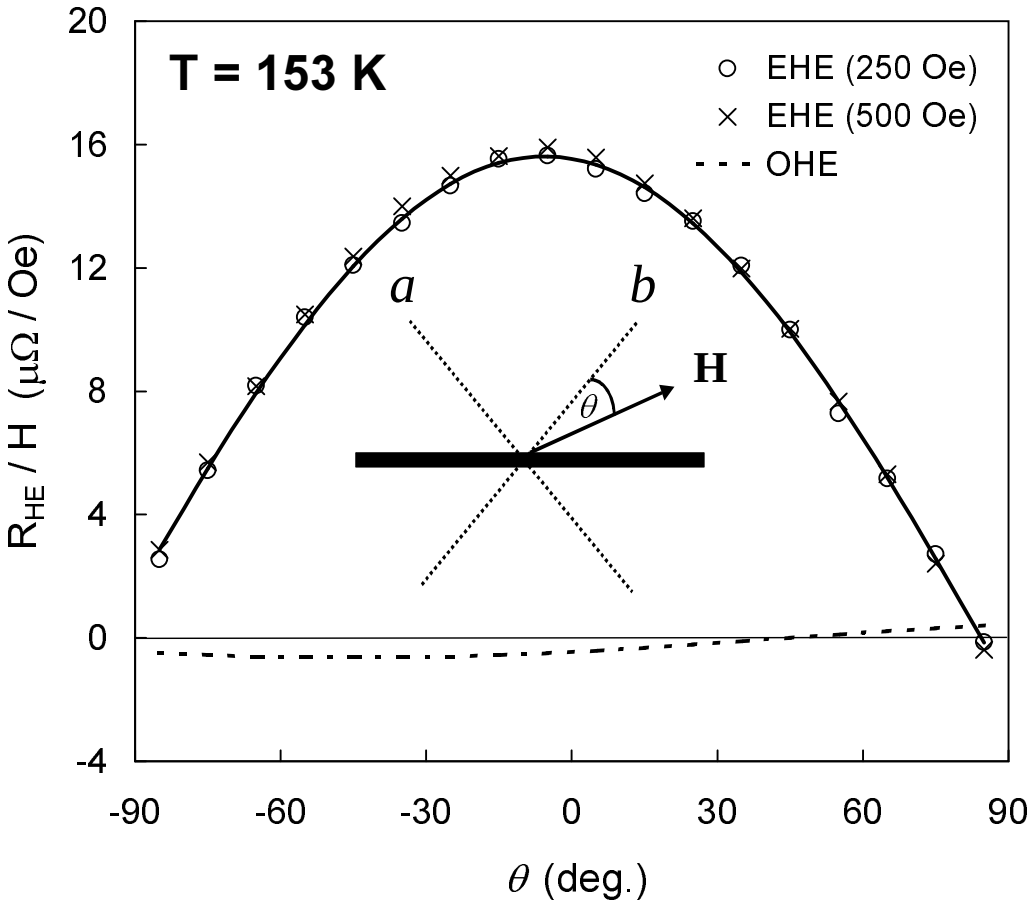

Figure 4.2: EHE at $T = 153$ K divided by the applied field H (circles: 250 Oe, crosses: 500 Oe) as a function of the angle θ between **H** and the b direction (see illustration). The dashed curve is the OHE. The solid curve is a fit obtained by assuming certain constant values for the susceptibility along the a and b directions.

the equation:

$$R_{EHE}(H,\theta) = \frac{R_s H}{\sqrt{2}t}\left(\chi_b \cos\theta - \chi_a \sin\theta\right). \tag{4.1}$$

Figure 4.2 also demonstrates the relatively small magnitude and different angular dependence of the OHE, which was subtracted from the measured signal.

Figure 4.3 presents the temperature dependence of the susceptibilities χ_a and χ_b (multiplied by R_s). We see that the susceptibility is very anisotropic throughout most

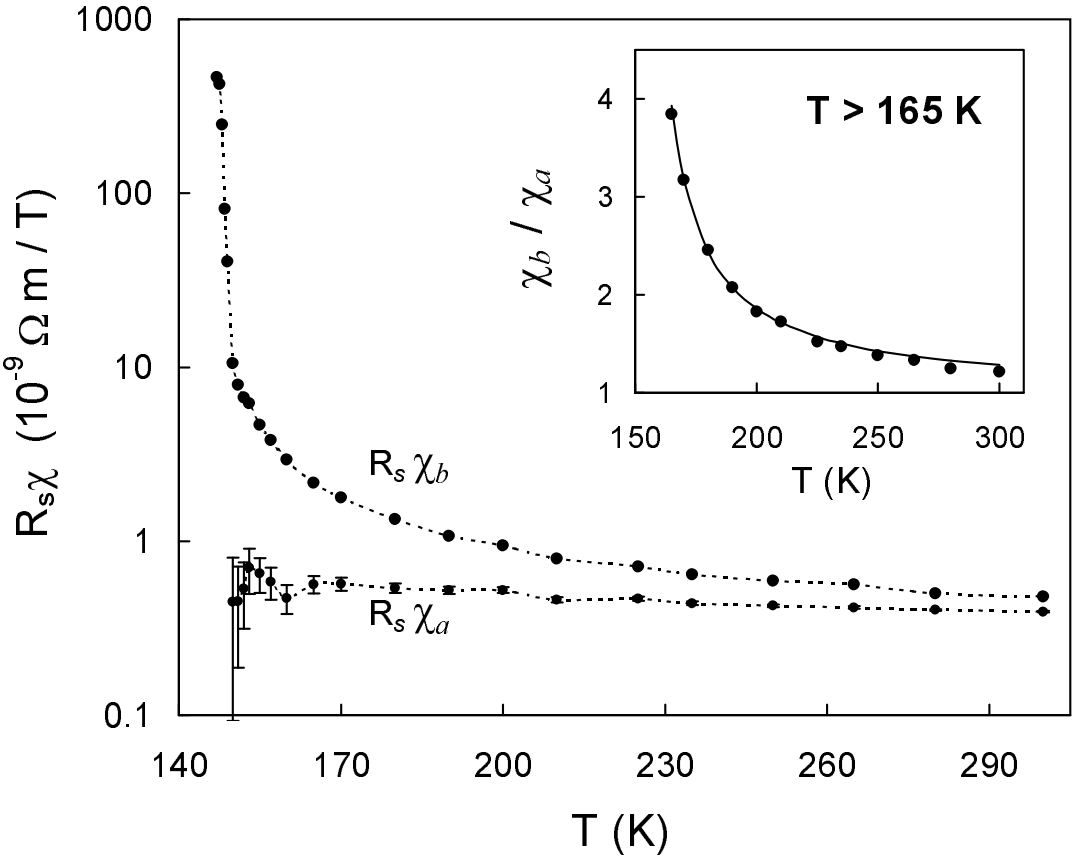

Figure 4.3: Susceptibility along the crystallographic directions [100] (χ_a) and [010] (χ_b) as a function of temperature, on a semilog plot. The values are multiplied by R_s, whose temperature dependence is expected to be smooth. The error bars for $R_s\chi_a$ reflect an uncertainty of up to 2° in θ. The dashed lines are guides to the eye. The inset shows the ratio χ_b/χ_a for 165 K $< T <$ 300 K. The solid curve is a fit to $\left(T - T_{c,a}^{MF}\right) / \left(T - T_{c,b}^{MF}\right)$ with $T_{c,a}^{MF} = 109$ K, $T_{c,b}^{MF} = 150.5$ K.

of the investigated temperature range. Particularly, χ_b exhibits striking divergence at T_c, while χ_a changes moderately. The actual divergence of χ_b is even stronger than shown in Fig. 4.3 since χ_b was not corrected for the demagnetizing field.[2]

[2]When an external field H_{ext} is applied along the easy axis, the total field along the easy axis is $H = H_{ext} - \frac{1}{2}\mu_0 M$ due to the demagnetization field (taking into account the 45° angle relative to the plane of the film). The apparent small-field susceptibility is $\chi_{meas} = \mu_0 M/H_{ext}$ while the real susceptibility is $\chi = \mu_0 M/H$. Therefore, the apparent susceptibility in our measurement configuration is only $\chi_b/(1 + \chi_b/2)$. A correction was not made because the value of R_s is not precisely known.

Since the c direction is in the plane of the film, the EHE measurement could not be used to determine χ_c (the insensitivity of EHE to a field component in the c direction was experimentally confirmed). Therefore, measurements of magnetoresistance (MR) $\Delta\rho \equiv \rho(H) - \rho(0)$ were employed. Based on the result presented in the inset to Fig. 4.4, as well as the analysis described in Appendix A, $\Delta\rho \propto -M^2$ (for a constant direction of magnetization). Thus we can infer the susceptibility behavior along a, b, and c directions by comparing the MR obtained with fields applied along these directions. The results, shown in Fig. 4.4, clearly indicate that the induced magnetization along the b direction grows as T_c is approached much more rapidly than along the a or c directions. The divergence in Fig. 4.4 is less pronounced than in Fig. 4.3 since for fields applied here the magnetization along b is sub-linear (but using lower fields would not allow us to obtain accurate MR data for the a and c directions). The temperature dependence of the MR with $\mathbf{H} \parallel c$ is very similar to the MR with $\mathbf{H} \parallel a$, indicating that the behavior of χ_c is similar to the behavior of χ_a.

4.4 Discussion: Anisotropy of the paramagnetic susceptibility

The data in Figs. 4.3 and 4.4 imply that only the susceptibility along the b direction (which is also the easy axis of the spontaneous magnetization) diverges at the phase transition; moreover, the large anisotropy of the susceptibility is noticeable

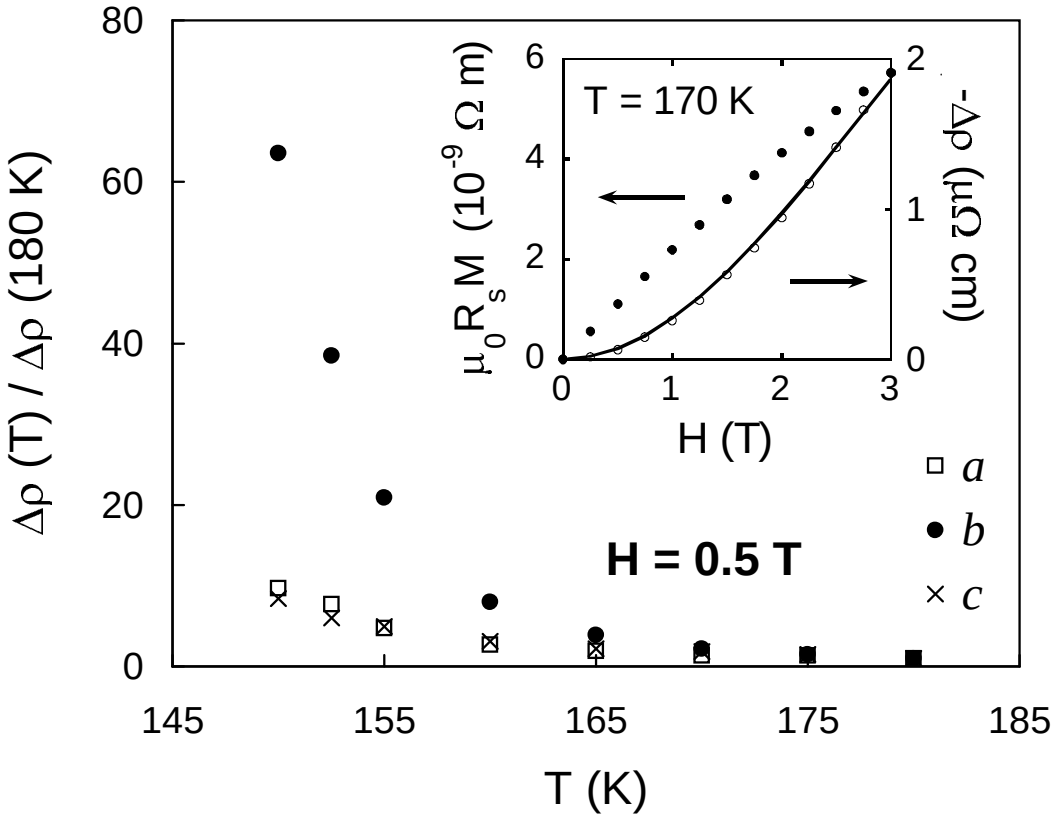

Figure 4.4: Magnetoresistance as a function of temperature with a field of 0.5 T applied along the different crystallographic directions (the values are normalized to the values at 180 K). The inset shows the magnetization ($\mu_0 R_s M$) and magnetoresistance ($\Delta\rho$) as a function of a field (applied along the b direction, at $T = 170$ K). The solid curve is a fit to $\Delta\rho \propto -M^2$.

($> 30\%$) already at $t \equiv (T - T_c)/T_c = 0.5$.

The coupling of spin to electronic orbitals yields the ubiquitous phenomenon of magnetocrystalline anisotropy (MCA) in ferromagnets [49]. While the manifestation of MCA below T_c in the form of hard and easy axes of magnetization is well studied, the fact that the strength of the MCA decreases with temperature as a high power of the spontaneous magnetization [50] could give the impression that MCA effects above T_c are at most a weak perturbation. Here we have shown that the MCA has a

significant effect in the paramagnetic state of the itinerant ferromagnet $SrRuO_3$ over a wide range of temperatures.

We note that this result is consistent with a previous work presented in Appendix A, where Ising-like critical behavior in $SrRuO_3$ films was detected.

Anisotropy in the behavior of the susceptibility arising from MCA may be described microscopically by Heisenberg model with *anisotropic exchange*:

$$\mathcal{H} = -\sum_{<ij>,\alpha} J_\alpha S_{i\alpha} S_{j\alpha} \tag{4.2}$$

or with *single-site anisotropy*:

$$\mathcal{H} = -J \sum_{<ij>} \mathbf{S}_i \cdot \mathbf{S}_j - \sum_{i,\alpha} D_\alpha S_{i\alpha}^2, \tag{4.3}$$

where $\alpha = a, b, c$ denotes spin components along the crystalline directions, and i, j denote lattice sites. $SrRuO_3$ is an itinerant ferromagnet. However, various theoretical models (e.g., the local-band theory mentioned in Sec. 1.2.4) indicate that magnetic moments in itinerant ferromagnets can behave as if localized even above T_c, thus vindicating the description of their magnetic interactions by Heisenberg Hamiltonian.

Since $T_c \propto J$, anisotropic exchange results in a different effective T_c for each spin component. Consequently, the susceptibility along the direction with the largest J diverges at the actual T_c, while no divergence occurs for the other spin components at any temperature [51]. Single-site anisotropy yields the same critical behavior [51], with an effective $\Delta J = \Delta D/z$, where z is the number of nearest neighbors.

The anisotropy ΔJ (or ΔD) can be estimated from the susceptibilities in the mean-field region, which are expected to follow the Curie-Weiss $1/\left(T - T_c^{MF}\right)$ law (with different mean-field transition temperature T_c^{MF} for each direction), if Pauli

paramagnetism and diamagnetism can be neglected.[3] We cannot fit $R_s\chi_a$ or $R_s\chi_b$ as a function of temperature because the temperature dependence of R_s is unknown. However, the ratio χ_b/χ_a does not depend on R_s, and fitting the data to the expression $\left(T - T_{c,a}^{MF}\right) / \left(T - T_{c,b}^{MF}\right)$ converges to the values $T_{c,a}^{MF} = 109\pm2$ K, $T_{c,b}^{MF} = 150.5\pm0.5$ K for 165 K $< T <$ 300 K (see inset in Fig. 4.3). From these values we find an anisotropy of $J_b - J_a = (0.33 \pm 0.05)J_{avg}$ or $D_b - D_a = (0.33 \pm 0.05)Jz$, where the error bars represent a possible variation of $\pm30\%$ in the OHE between 127 and 300 K.

Direct measurements of magnetization of films in the ferromagnetic phase show that at low temperatures the rotation of $\mathbf{M}$ in the (001) plane can be described by an anisotropy energy, $E_{anis} = K\sin^2\theta$, with an anisotropy constant $K = (1.2 \pm 0.1) \times 10^7$ erg/cm^3 [35, 36]. To relate the ferromagnetic anisotropy with Eqs. (4.2) and (4.3), we note that at low temperatures the exchange aligns the spins along a single direction; thus, the energy cost of magnetization rotation from the b direction toward the a direction by an angle θ in the case of anisotropic exchange is $\Delta E = zNS^2(J_b - J_a)\sin^2\theta$, where N is the number of spins per unit volume. A similar result is obtained in the case of single-site anisotropy. Calculating J according to the relation $J = 3k_BT_c^{MF}/2zS\,(S+1)$ we obtain $J_b - J_a \simeq 0.1J_{avg}$. This result is in reasonable agreement with $J_b - J_a = (0.33 \pm 0.05)J_{avg}$ extracted from the anisotropic susceptibility, in view of the uncertainties involved.[4]

[3]The Pauli paramagnetism and diamagnetism in $SrRuO_3$ are approximately 10% of the susceptibility at 300 K [52]. It is not clear whether their contribution to the EHE should go with the same R_s. If same R_s is assumed, taking them into account does not have a significant effect on the result or the quality of the fit.

[4]The slow change in the direction of the easy axis as a function of temperature (see Sec. 1.2.4) indicates an imperfectness of the model; due to the itineracy of the magnetic moments, it is not

A paramagnetic susceptibility diverging along only one crystallographic direction has been reported previously for bulk specimens of $Cu(NH_4)Br_4 \cdot 2H_2O$ [53], but the anisotropy there was found to be only 2% of the exchange integral J (compared to 33% which we find in $SrRuO_3$). Another report refers to two-dimensional cobalt films, where an anisotropy of 5% was measured [54]. In both cases, the temperature range for which the susceptibility was measured is by an order of magnitude smaller (in units of T_c) than in our measurements of the three-dimensional $SrRuO_3$ films.

It should be noted that measuring paramagnetic susceptibility in films often poses a considerable technical challenge due to the combination of small magnetic moment of the film with large background signal from the substrate. However, the use of EHE avoids these difficulties, since the EHE depends on the film internal magnetization and not on the total magnetic moment of the sample. Therefore, the signal does not diminish with decreasing thickness, neither is it affected by the substrate magnetization.

---

really clear which values should be substituted for N and S; the temperature dependence of the band structure is neglected in our analysis; there might be a mistake in the subtracted value of the OHE due to EHE anisotropy (see Sec. 5.3).

4.5 Discussion: EHE in the paramagnetic state

The results of our experiment provide information regarding the temperature dependence of R_s in $SrRuO_3$ above T_c, complementing the data for $T < T_c$ reported previously. Up to a constant prefactor, R_s can be inferred from the fit in the inset of Fig. 4.3 (assuming Curie-Weiss behavior for the susceptibilities). We estimated the prefactor (with an uncertainty of about 15%) by using the relation between MR and M established in Appendix A. The results are shown in Fig. 4.5.

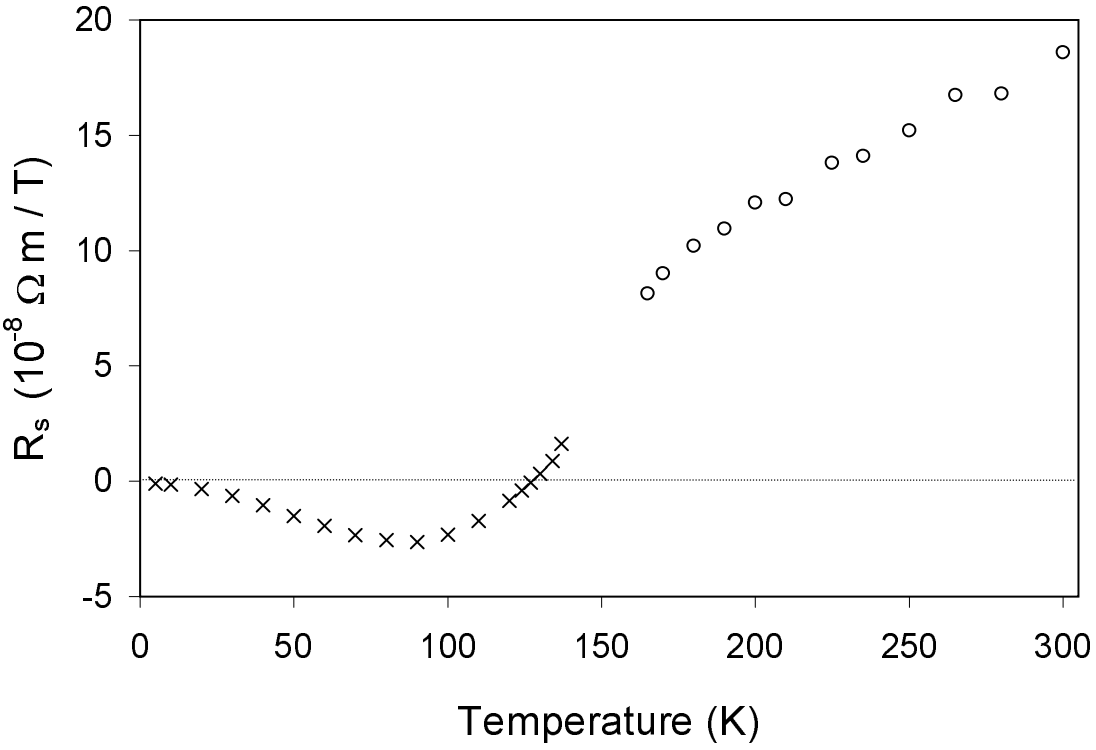

Figure 4.5: EHE coefficient R_s as a function of temperature. The crosses represent previously known data from the ferromagnetic phase, and the circles represent new data from the paramagnetic phase.

Above T_c, R_s is positive (unlike throughout most of the temperature range below

T_c) and it steadily increases as a function of temperature, continuing the trend which started below T_c. The dependence of R_s on the resistivity ρ in this range of temperatures is roughly quadratic, as shown in Fig. 4.6. These results will need to be taken into account in any new attempt to calculate the EHE in $SrRuO_3$.

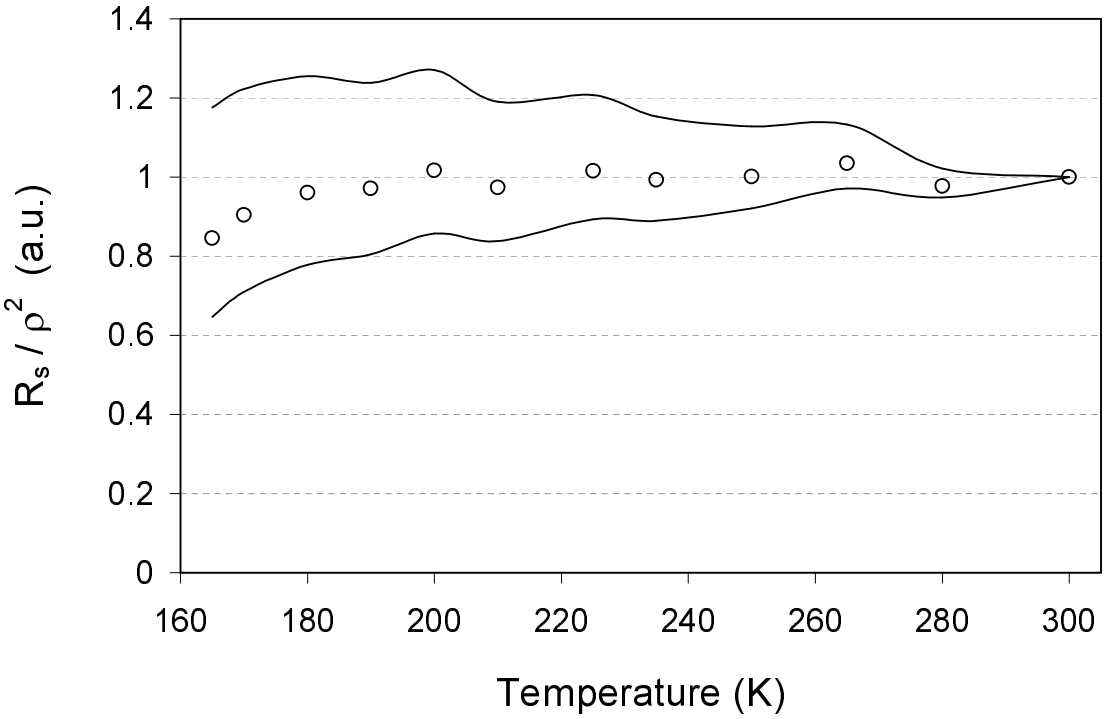

Figure 4.6: The circles represent R_s/ρ^2 (all values are normalized to the value at 300 K). The solid curves indicate how the results will change if the OHE is not constant, but changes by $\pm 30\%$ from 127 K (where it was measured) to 300 K.

Chapter 5

Anisotropy of the EHE

5.1 Experiment

Commonly, it is assumed that the EHE is determined by the component of **M** which is perpendicular to the measurement plane ($M_\perp$). We found a deviation from this behavior in $SrRuO_3$, as described below.

In the following experiment, Hall effect is measured in the ferromagnetic state ($T = 90$ K) while the magnetic field is applied in the plane of the film, thus avoiding the OHE contribution (due to purely geometrical reasons).[1] The magnetic field rotates the magnetization from an angle of 39° relative to the normal towards the plane of the film, making $M_\perp$ smaller. Since the spontaneous magnetization at this

[1]There might be still an OHE contribution due to an uncertainty in the angle setting, and its possible effect is shown below. This uncertainty also prevents an accurate characterization of temperature dependence of the effect, since the EHE is smaller at much lower or much higher temperatures, so that the effect of the unwanted OHE contribution (which is roughly temperature independent) becomes more significant.

temperature is nearly 80% of the zero-temperature magnetization, the applied field practically does not change its *magnitude*, as confirmed by direct measurements of the magnetization [35]. As a result, the measured EHE is expected to decrease as a function of the magnetic field due to the $\hat{\mathbf{m}} \cdot \hat{\mathbf{n}}$ factor in Eq. (1.4).

5.2 Results and discussion

A decrease in the EHE as a function of H is indeed observed. However, when compared with measurements of magnetization in SQUID with the same direction of the magnetic field [35], a quantitative disagreement appears. For example, according to the SQUID data, when $H = 5$ T is applied, $M_\perp$ decreases by 25% due to the rotation of the magnetization (while the magnetization rotates by 15°). However, according to the Hall effect data, the EHE (which is assumed to be proportional to $R_s M_\perp$) decreases by only (8 ± 2)%. The results of both types of measurements are shown in Fig. 5.1.

The discrepancy cannot be attributed to a resistivity-dependent change in R_s as a function of the field due to the magnetoresistance. In order to explain the discrepancy by this effect, $|R_s|$ at $H = 5$ T should increase by about 20% relative to its zero-field value. On the contrary, the MR at $H = 5$ T is -7%, which should result in a 4% *decrease* in $|R_s|$, based on the temperature-dependent variation of R_s.

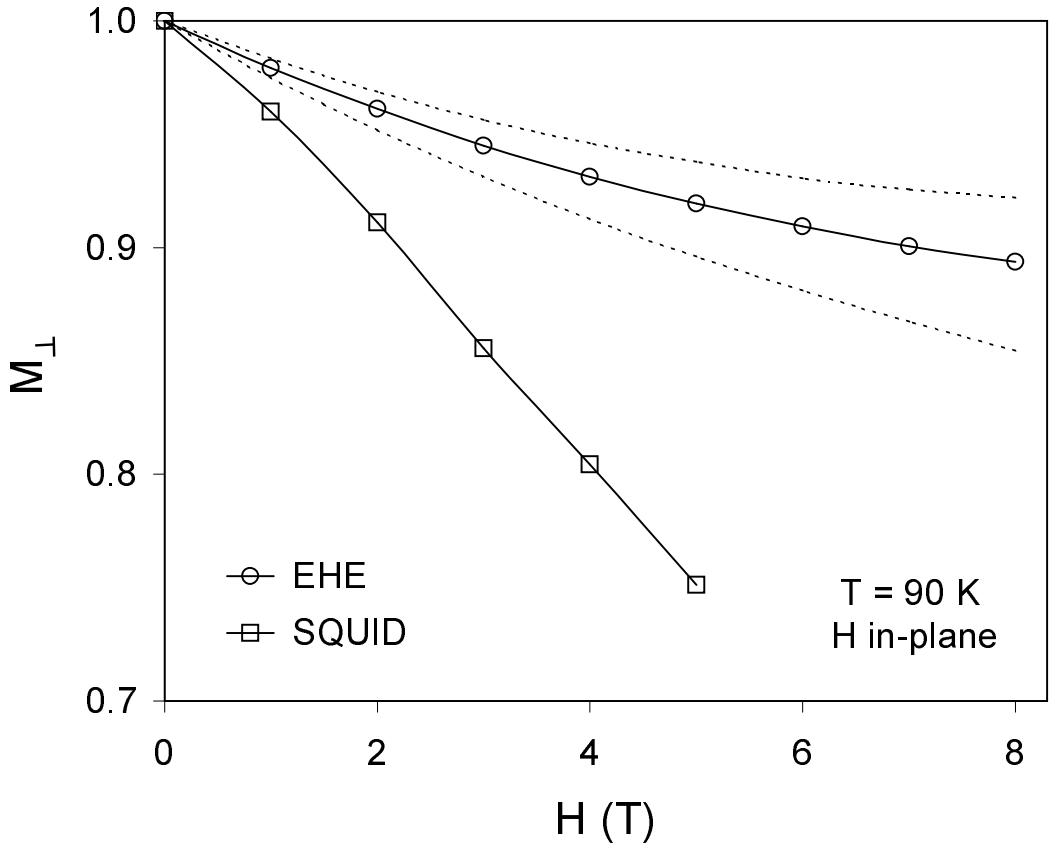

Figure 5.1: The perpendicular component of the magnetization $M_\perp$ as a function of the in-plane magnetic field H, as determined from measurements of EHE (circles) and from measurements of magnetization in SQUID (squares). (The values are normalized to the zero-field value.) The dashed curves demonstrate the error due to a 2° uncertainty in the angle setting.

It should be noted that it would be even more difficult to reconcile the results with the Berry phase model which would predict a 35% decrease in the EHE for $H = 5$ T (due to a 25% decrease in $\hat{\mathbf{m}} \cdot \hat{\mathbf{n}}$ and a 14% decrease in ρ^2), instead of the observed 8% decrease.

We interpret this result as an evidence for the dependence of the EHE coefficient R_s in $SrRuO_3$ on the direction of $\mathbf{M}$ relative to the crystalline directions. Our results

correspond to a change in R_s of nearly 20% due to a rotation of 15°.

To our best knowledge, anisotropic EHE has never been reported for any material. However, there is no reason to exclude this possibility, particularly in view of the anisotropy of the magnetoresistance (see Sec. 1.2.5).

On the other hand, there is a very little dependence of the EHE on the direction of the current (not shown).

5.3 Relevance to other parts of this work

In the interpretation of the susceptibility anisotropy (Fig. 4.3), it was assumed that R_s has the same value for a magnetization along the a and b crystalline directions. The observed 3-orders-of-magnitude difference between $R_s\chi_a$ and $R_s\chi_b$ near T_c could be affected very little by the EHE anisotropy. On the other hand, the value of ΔJ determined from the results may be affected. However, since the measurements there were performed in the zero-magnetization limit, the EHE anisotropy should be partly averaged out because the orientations of the moments relative to the crystalline axes are not fixed in the direction of the magnetization as in the ferromagnetic state, but they are distributed in space, and only a small deviation from this distribution creates the magnetization. This results in an effective R_s which is not equal to the R_s which corresponds to the actual direction of the magnetization, but depends also on the

zero-field distribution of the directions of the magnetic moments (and the values of R_s corresponding to those directions). In addition, the observed tendency of $R_s\chi_a$ and $R_s\chi_b$ to coincide in the high temperature limit indicates that the EHE anisotropy is not large. Still, the extracted value of ΔJ could be affected by the effect of EHE anisotropy on the OHE measurement, which is discussed below.

The identification of the OHE by the experiment presented in Sec. 2.3.3 might be inaccurate if the EHE is anisotropic. In that experiment the magnetization deviates from the easy axis by a small angle

$$\Delta\alpha_M \simeq \frac{MH}{2K}\sin(\alpha - \alpha_{ea}). \tag{5.1}$$

In the case of an anisotropic EHE, this would create an additional contribution to the field-induced EHE of the form

$$\Delta\rho_{xy} = \frac{\partial\rho_{xy}^{EHE}}{\partial\alpha_M}\Delta\alpha_M \tag{5.2}$$

$$\simeq \frac{\partial\rho_{xy}^{EHE}}{\partial\alpha_M}\frac{MH}{2K}\left(\cos\alpha_{ea}\sin\alpha - \sin\alpha_{ea}\cos\alpha\right). \tag{5.3}$$

This contribution has the same dependence on H and α as the expression in Eq. (2.3), therefore it cannot be detected just by inspection of the data. However, we can calculate whether $\partial\rho_{xy}^{EHE}/\partial\alpha_M$ may be large enough to create a significant error in the OHE, thus questioning some of our results, among them the conclusion regarding the inapplicability of the Berry phase theory (Chapter 3).

As can be seen from Fig. 3.1, if the OHE were approximately zero (compared to its assumed value), the EHE would vanish at a correct field to agree with the Berry phase theory. In order to get $R_0 = 0$ from the fit in Eq. (2.3), it would be needed to have $\partial\rho_{xy}^{EHE}/\partial\alpha_M \simeq 9$ nΩ cm/$^\circ$. This would imply that the EHE is so anisotropic

that a hypothetical rotation of $\mathbf{M}$ by roughly 60° would change ρ_{xy} at $T = 127$ K from 0 to the maximal value it reaches in Fig. 1.4. We consider such drastic change to be unlikely (although we cannot exclude it altogether).

A smaller error in the OHE could affect the various quantitative results presented in this thesis. However, the results will not change significantly due to such error, as they did not change much due to an assumption of a 30% temperature-dependent change in the OHE.

Chapter 6

Summary

We investigated thin films of $SrRuO_3$ by measurements of Hall effect combined with measurements of resistivity and in some cases confronted with measurements of magnetization, as a function of temperature and magnetic field.

While commonly the behavior of the EHE is characterized by measuring its temperature dependence, we presented measurements of the EHE in $SrRuO_3$ as a function of the magnetic field. This gives a new degree of freedom for studying the EHE. In our case, these measurements provided a clear indication that the EHE in $SrRuO_3$ should be described in terms of a ρ-dependent R_s and not an M-dependent σ_{xy}.

In addition, we extended the range of resistivities for which R_s has been measured in $SrRuO_3$ by performing measurements in the paramagnetic phase. These results will need to be taken into account in any future theoretical explanation for the EHE in this material.

We also presented an observation showing that the EHE in $SrRuO_3$ has a non-trivial dependence on the direction of $\mathbf{M}$ relative to the crystalline directions. To our best knowledge, there are no experiments on other materials confirming or excluding a behavior of this kind.

While it is common to use the EHE as an indicator of magnetization, it is seldom used for a quantitative analysis of magnetic behavior. In this work we presented a striking example of the latter, by performing sensitive measurements of the zero-field magnetic susceptibility in $SrRuO_3$ films, which allowed us to gain a unique insight into the effect of the magnetocrystalline anisotropy in the paramagnetic state of an itinerant ferromagnet.

Appendix A

Magnetic Resistivity and the Ferromagnetic Phase Transition

Note:

The results described in this Appendix have been published in:

Y. Kats *et al.*, Phys. Rev. B **63**, 054435 (2001).

A.1 Experiment

We measured the electrical resistivity of $SrRuO_3$ as a function of temperature and magnetic field near the ferromagnetic phase transition ($T_c \sim 153$ K).

Assuming that the resistivity can be separated into magnetic (i.e., related to spin scattering) and non-magnetic parts, the application of a magnetic field in the range of temperatures $120 - 180$ K is expected to affect the magnetic part while its effect on the non-magnetic part (through the Lorentz force) is expected to be negligible due to

the relatively short mean free path in $SrRuO_3$ at these temperatures.[1] Consequently, field-induced changes in resistivity are directly related to the induced changes in magnetization.

The magnetic field **H** was applied along the easy axis of magnetization (the [010] direction) in order to avoid changes in the direction of **M** which could induce changes in resistivity due to the anisotropic magnetoresistance (see Sec. 1.2.5), and to avoid the effect of the magnetocrystalline anisotropy which otherwise would compete with the applied field and complicate the relation between the magnitudes of **M** and **H**. The current was parallel to the [001] direction.

Measurements below T_c were done with the sample uniformly magnetized (see Sec. 2.3.1). Thus, they do not involve effects of changes in the domain structure or domain-wall resistivity [55], but reflect solely the changes in the intrinsic magnetization.

The film whose results are presented below has a thickness of 200 nm, and $T_c \simeq 153$ K.

[1] From Ref. [19], the Fermi velocity is $\sim 2 \times 10^7$ cm/s and the mean free path is of order of 10 Å, thus the quasiparticle scattering time is $\tau \sim 5 \times 10^{-15}$ s. Calculating the cyclotron frequency ω_c (taking the cyclotron mass to be $0.2m_e$, as found from quantum oscillations measurements [25]), we find $(\omega_c\tau)^2$ to be $3-4$ orders of magnitude smaller than the measured relative magnetoresistances $\Delta\rho/\rho$.

A.2 Data analysis

A.2.1 Zero-field resistivity and the critical exponent β

The zero-field resistivity near T_c is shown in Fig. A.1. Since above T_c the magnetization vanishes, the magnetic resistivity induced by spin scattering is expected to become temperature-independent far enough above T_c. Therefore, we may assume that the temperature dependence of the resistivity there is only due to non-magnetic components of the resistivity. Assuming that the behavior of the *non-magnetic* resistivity is not affected by the ferromagnetic phase transition, its behavior below T_c can be approximated (in some small range of temperatures) by an extrapolation of the resistivity above T_c, which we denote by $\rho^+(T)$. We then subtract the measured resistivity below T_c from the extrapolated $\rho^+(T)$ (based on a linear fit of the range $160 - 170$ K) and denote the difference by $\Delta\rho_{sp}$ (see Fig. A.1). This difference is related to magnetic ordering, and in the following we determine its functional dependence on the magnetization M.

Figure A.2 shows a plot of $\ln \Delta\rho_{sp}$ as a function of $\ln |t|$, where $t = (T - T_c)/T_c$, and $T_c = 153$ K. The temperature range used in this fit is 130 K - 149 K. The linearity of the plot in Fig. A.2 clearly indicates that $\Delta\rho_{sp}$ exhibits a power-law behavior as a function of $|t|$:

$$\Delta\rho_{sp} \propto |t|^s \tag{A.1}$$

where $s = 0.68$ is the slope of the plot.

If the magnetic resistivity ρ_m depends only on the magnetic ordering, we can expand the magnetic resistivity in a power series in M around $\rho_m(0)$, which is the magnetic resistivity when no magnetic order exists. Due to symmetry, only even

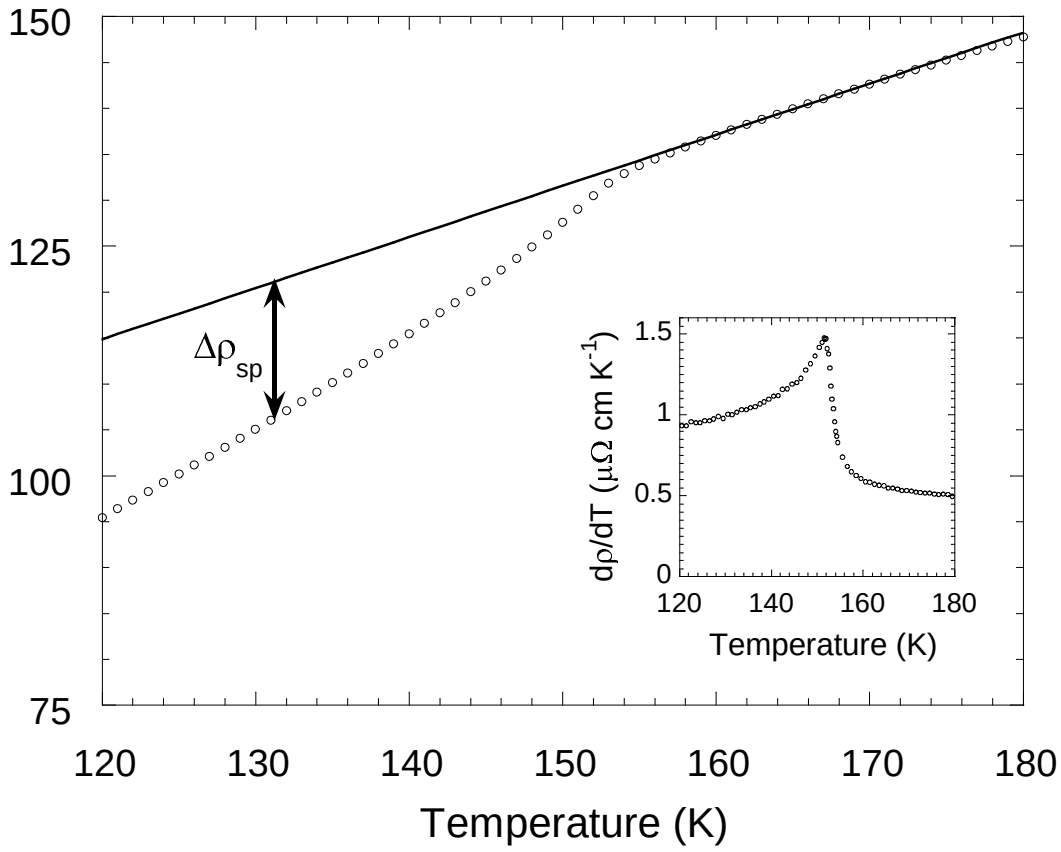

Figure A.1: Temperature dependence of zero-field resistivity ρ near T_c ($\sim$ 153 K). The solid line is the extrapolation of the resistivity from $T > T_c$. The definition of $\Delta\rho_{sp}$ is shown. The inset shows the behavior of $d\rho/dT$.

powers of M appear in the expansion:

$$\rho_m(M) = \rho_m(0) - aM^2 - bM^4 + \cdots . \tag{A.2}$$

On the other hand, we assume that $\Delta\rho_{sp}$ is simply:

$$\Delta\rho_{sp}(T) = \rho_m(0) - \rho_m(M_{sp}(T)), \tag{A.3}$$

where $M_{sp}(T)$ is the spontaneous magnetization. Thus we obtain

$$\Delta\rho_{sp} = aM_{sp}^2 + bM_{sp}^4 + \cdots \tag{A.4}$$

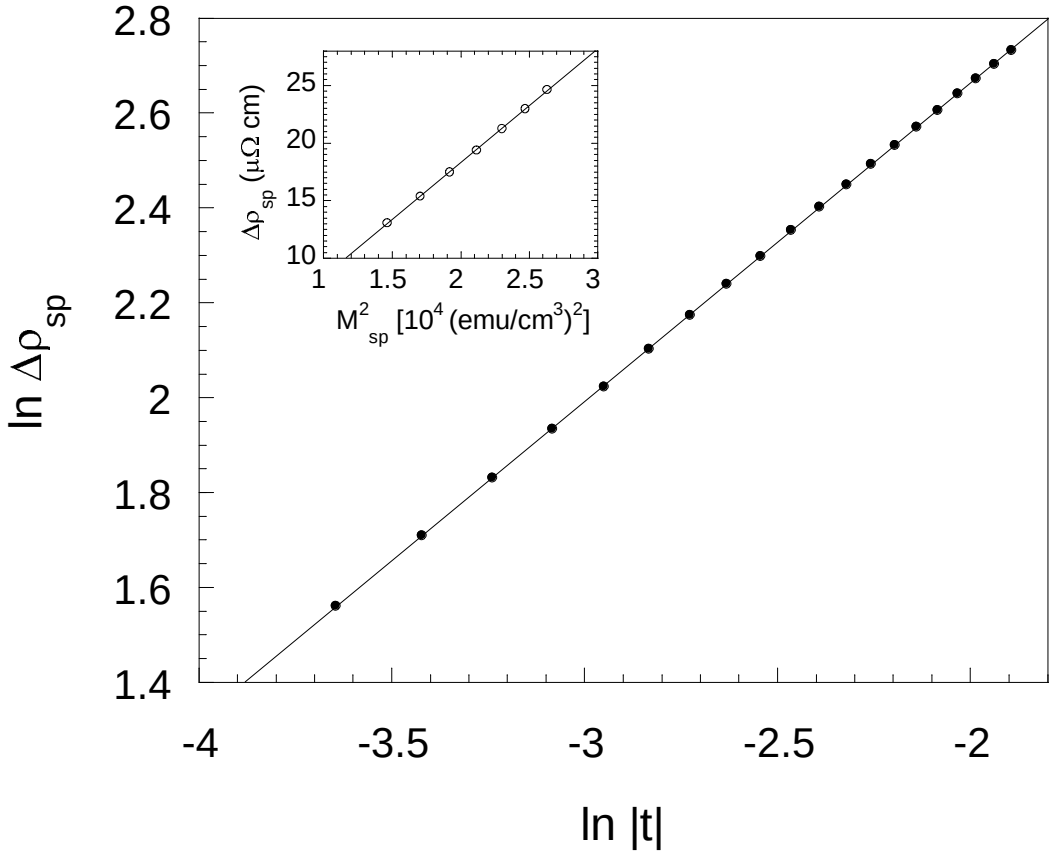

Figure A.2: Critical behavior of $\Delta\rho_{sp}$ with respect to the reduced temperature $t = (T - T_c)/T_c$ from 130 to 149 K with $T_c = 153$ K. A linear fit is shown. The inset shows the correspondence between $\Delta\rho_{sp}$ and the square of the measured spontaneous magnetization M_{sp}.

In the vicinity of the critical point, M_{sp} is expected to exhibit a power-law behavior of the form $M_{sp} \propto |t|^{\beta}$. Therefore we suggest, on the basis of the result in Eq. (A.1), that in our case $\Delta\rho_{sp}$ is well described by the first term alone of Eq. (A.4) and then it follows that

$$\Delta\rho_{sp} \propto |t|^{2\beta} \tag{A.5}$$

where β is the critical exponent of the magnetization.

This implies that β can be found from a plot of $\ln \Delta\rho_{sp}$ as a function of $\ln |t|$,

as in Fig. A.2. Hence we obtain $\beta = 0.34$, which is a reasonable value for this exponent. (Usually β is found to have values between 0.3 and 0.5. See, e.g., Refs. [56, 57, 58, 59]).

For a reliable analysis, it is necessary to accurately determine the value of T_c. It can be found from the location of the peak of $d\rho/dT$ (denoted hereafter by T_c'), and from the location of the peak of the induced magnetization at a constant magnetic field (hereafter denoted T_c''). Ideally, $T_c = T_c' = T_c''$; however there is always some smearing of the transition (due to, e.g., defects or small temperature gradients), which may slightly shift T_c' and T_c'' relative to T_c.

We find that $T_c' = 152$ K. However, since $d\rho/dT$ decreases above T_c much faster than it grows below T_c (see inset to Fig. A.1), it is clear that rounding of the ideal $d\rho/dT$ *vs.* T (caused by the smearing) would result in a negative shift of T_c', namely, $T_c' < T_c$.

We estimate T_c'' to be the location of the maximum of the (negative) magnetoresistance at a constant field. We find that $T_c'' = 153.5 \pm 0.7$ K. However, due to the smearing, we expect to obtain $T_c'' > T_c$. This is because the critical susceptibility above T_c has a larger amplitude than it has below T_c (see values of C^+/C^- in Table A.1).

Based on these results and considerations, we conclude that the value of $T_c = 153$ K which was used above is acceptable.

To determine more accurately the values of T_c and β we plotted $\Delta\rho_{sp}^{1/(2\beta)}$ as a function of T for trial values of β until the best linear dependence was obtained. From the intercept of the line with the T axis we found T_c. Our basic choice is to

make the extrapolation of $\rho^+(T)$ upon the range of $160 - 170$ K (not too far from the investigated area and not too close to T_c) and to make the fit of $\Delta\rho_{sp}$ between $140 - 149$ K (not too far from T_c, so that only the leading asymptotic terms are significant, and not too close to T_c, so that the results are not affected by the smearing and by the short-range spin correlations). This results in $T_c = 153.2$ K and $\beta = 0.347$.

To check how a change of the fit range may affect the results we did the same calculation for the ranges $135 - 145$ K and $145 - 151$ K and obtained the results $T_c = 152.5$ K, $\beta = 0.325$ and $T_c = 153.4$ K, $\beta = 0.353$ for those ranges, respectively.

Another check was to change the range upon which the extrapolation of $\rho^+(T)$ is done. For a range of $160 - 180$ K we obtained $T_c = 153.4$ K, $\beta = 0.348$.

Therefore we conclude that reliable values are $T_c = 153.0 \pm 0.5$ K and $\beta = 0.34 \pm 0.02$.

Comparing these measurements with measurements of spontaneous magnetization on the same film we find that $\Delta\rho_{sp} = aM_{sp}^2$ (see inset to Fig. A.2) with $a = (9.5 \pm 1.0) \times 10^{-4} \frac{\mu\Omega\, cm}{(emu/cm^3)^2}$. After checking resistivities of other films, with different thicknesses ($100 - 2000$ Å) and different residual resistivities ($5 - 150$ $\mu\Omega$ cm), we find that the value of a is quite insensitive to these parameters (the observed changes were less than 20%).

A.2.2 Magnetoresistance and the critical exponent γ

The previous subsection implies that

$$\rho_m(M) = \rho_m(0) - aM^2. \tag{A.6}$$

This relation enables us to find the magnetic susceptibility from the measurements of magnetoresistance (i.e., the change in the resistivity upon application of field).

The initial susceptibility χ_0 (defined as $\partial M/\partial H$ at $H = 0$) is expected to exhibit a power-law behavior near T_c:

$$\chi_0 = C^{\pm} |t|^{-\gamma} \tag{A.7}$$

where C^+ and C^- are the amplitudes above and below T_c, respectively, and γ is the critical exponent. In the following we determine γ separately from measurements above and below T_c, and calculate the value of the amplitude ratio C^+/C^-.

Determination of γ above T_c:

We can expand the magnetic field H (at a constant temperature) as a power series in M:

$$H = a_1 M + a_2 M^3 + \cdots, \tag{A.8}$$

where a_1 and a_2 are temperature-dependent constants. For small fields, when the first two terms of the expansion are sufficient, we obtain

$$\frac{H}{M} = a_1 + a_2 M^2. \tag{A.9}$$

For $M \to 0$, Eq. (A.9) reduces to: $a_1 = H/M$. Therefore from the definition of the initial susceptibility χ_0 it follows that $\chi_0(T) = 1/a_1(T)$. We determine M from measurements of magnetoresistance according to Eq. (A.6). When plotting M^2 *vs.* H/M, the values of $a_1(T)$ can be found from the intercept with the H/M axis. Then the critical exponent γ is found from the slope of a log-log plot of χ_0 *vs.* $|t|$, according to the definition of γ in Eq. (A.7); see Fig. A.3. The plot includes the temperatures $155 - 166$ K. The value of γ found by this method is $\gamma = 1.17 \pm 0.14$.

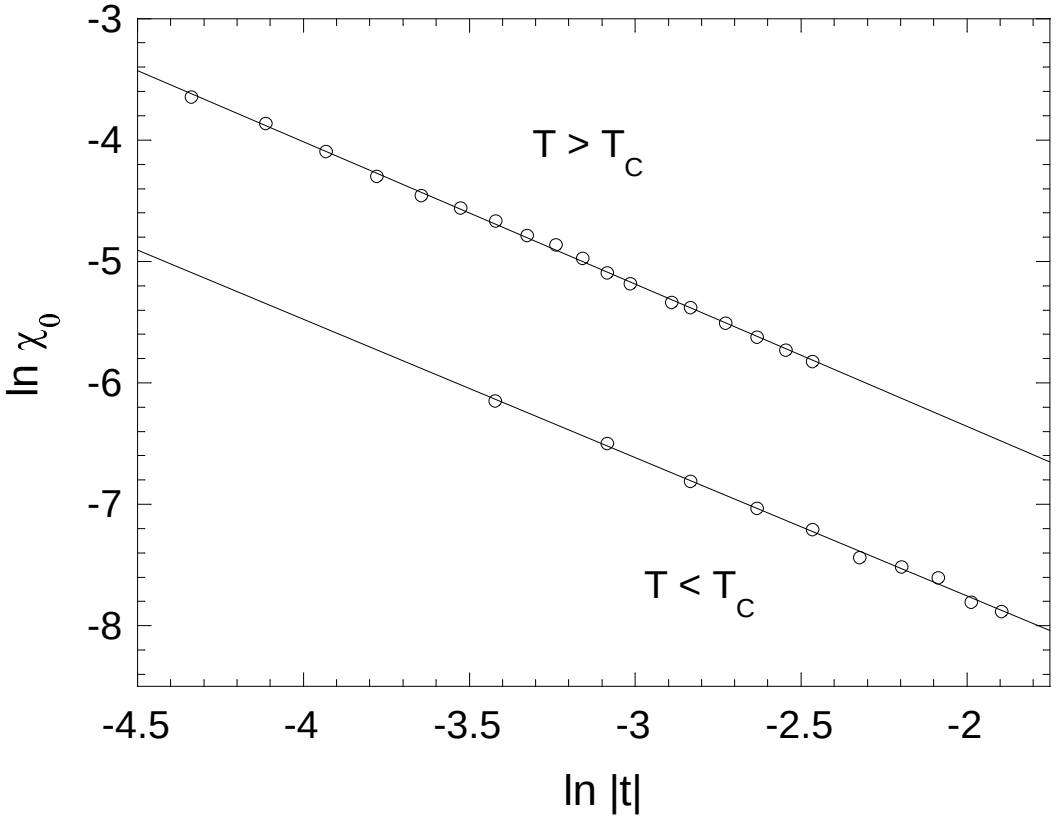

Figure A.3: Critical behavior of the initial susceptibility χ_0 below and above T_c. The critical exponent γ is found from the slopes of the linear fits.

Determination of γ below T_c:

Below T_c a linear response of the resistivity to a low magnetic field is observed. Thus $\partial M/\partial H$ at low fields is the initial susceptibility χ_0. The quantity $\partial M/\partial H$ can be found from the measured $\partial\rho/\partial H$, since using Eq. (A.6) we can write

$$\frac{\partial \rho}{\partial H} = -2aM_{sp}\frac{\partial M}{\partial H} \tag{A.10}$$

where the value of M_{sp} at each temperature can be obtained from the measurements of $\Delta\rho_{sp}$ (based on the relation $\Delta\rho_{sp} = aM_{sp}^2$). We calculated $\partial\rho/\partial H$ from measurements between $130 - 148$ K. At each temperature we used the range of magnetoresistances

from 0.08 to 0.16 $\mu\Omega\,$cm, where the fields were small enough so that $\partial M/\partial H$ is approximately χ_0, and high enough so that even at temperatures close to T_c they are higher than the fields where magnetization reversal starts. The value of γ found from the slope of a log-log plot of χ_0 *vs.* $|t|$ (see Fig. A.3) is $\gamma = 1.14 \pm 0.07$.

By comparing the susceptibilities above and below T_c we find that the amplitude ratio C^+/C^- is ~ 4.

The effect of the demagnetizing field was included in the analyses;[2] however the correction was usually small.

A.2.3 Magnetoresistance data collapse

According to the scaling law hypothesis, the relation between the magnetic field H, the magnetization M, and the reduced temperature t in the critical region has the form

$$\frac{M}{|t|^\beta} = f_\pm\left(\frac{H}{|t|^{\beta+\gamma}}\right) \tag{A.11}$$

where $f_\pm$ is a function that is different below and above T_c. Using Eq. (A.6) we obtain for the magnetoresistance

$$\begin{aligned} \Delta\rho(T,H) &= \rho(T,H) - \rho(T,0) \\ &= -a(M^2(T,H) - M^2(T,0)) \end{aligned}$$

[2]In our experiment, the magnetization has an angle of $\theta = 45°$ relative to the plane of the film. The in-plane component of M is perpendicular to the long dimension of the sample. Since the width-to-thickness ratio is large (~ 500), the demagnetization field due to the in-plane component is negligibly small, and the demagnetizing factor for the normal component is 4π. Therefore the demagnetizing field is $4\pi M \sin\theta$. It has a component in the direction of the easy axis and another component perpendicular to it. Magnetic field which is applied perpendicularly to the easy axis, has a very small effect on the magnetization because of the large magnetic anisotropy. Therefore we take only the component parallel to the easy axis as the effective demagnetizing field. Hence the correction should be $H = H_{ext} - 4\pi M \sin^2\theta$, where H_{ext} is the applied field.

$$= -at^{2\beta}\left[f_{\pm}\left(\frac{H}{|t|^{\beta+\gamma}}\right) - f_{\pm}(0)\right]$$

The expression within the square brackets is a function of $H/|t|^{\beta+\gamma}$ alone, therefore there exists a scaling law for the magnetoresistance of the form:

$$\frac{\Delta\rho}{|t|^{2\beta}} = F_{\pm}\left(\frac{H}{|t|^{\beta+\gamma}}\right) \tag{A.12}$$

or

$$r = F_{\pm}(h) \tag{A.13}$$

where $r = |\Delta\rho|/|t|^{2\beta}$ and $h = H/|t|^{\beta+\gamma}$. When the correct values of β and γ are substituted, plotting the values of r as a function of h should give a smooth curve (with two branches, described by F_+ and F_-, for $T > T_c$ and $T < T_c$, respectively). The correction of the applied field for the demagnetization was not taken into account here.

Figure A.4 shows the data collapse obtained with the values of the critical exponents and T_c found above ($T_c = 153$ K, $\beta = 0.34$ and $\gamma = 1.15$). This plot includes data for temperatures between 130 K and 170 K (excluding the temperatures $|T - T_c| < 3$ K) and fields between 2 and 10 kOe. It is clearly seen that measurements at different temperatures fall on the same curve.

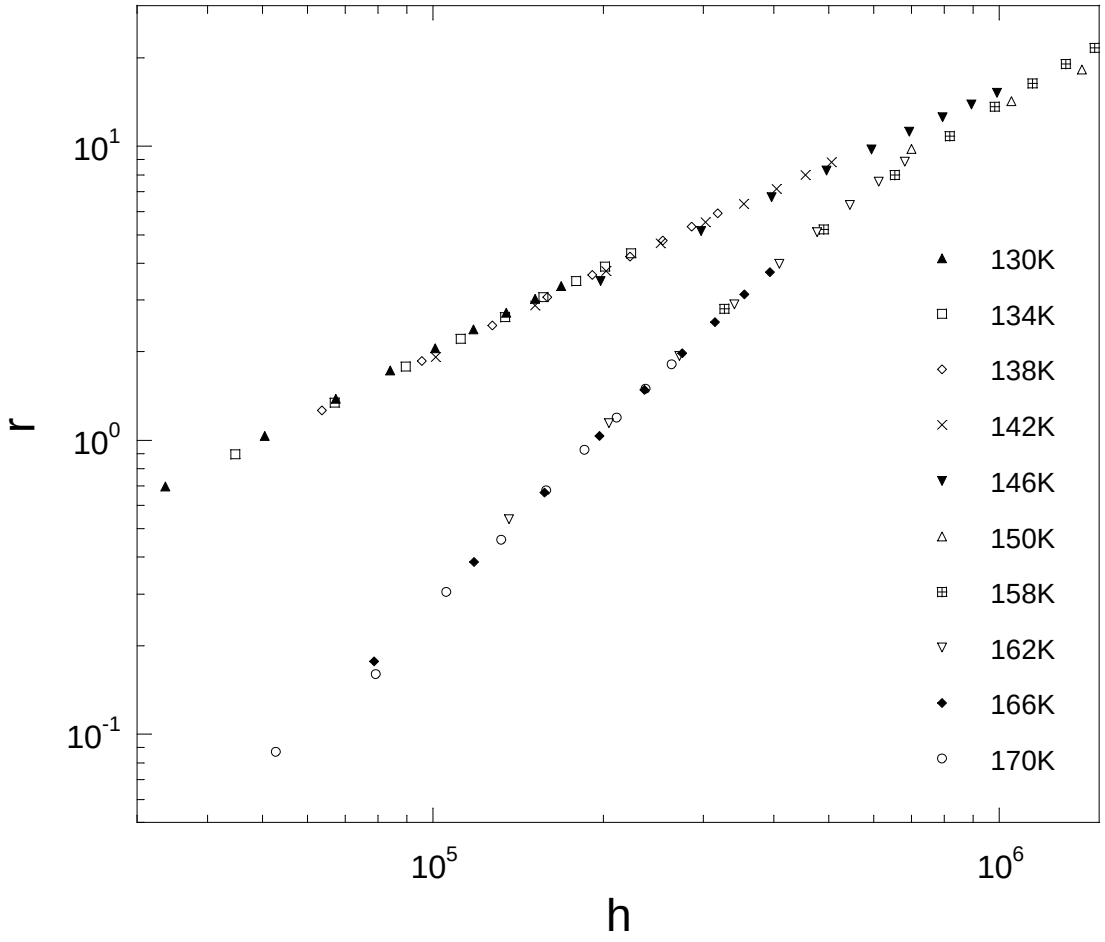

Figure A.4: Scaling of the magnetoresistance-temperature-field data. The quantities r and h are defined in the text. Data for fields between 2 and 10 kOe and temperatures between 130 and 170 K, see legend, is included.

A.3 Summary and conclusions

From the behavior of the zero-field resistivity near the ferromagnetic phase transition we concluded that the dependence of the magnetic resistivity on the magnetization is: $\rho_m(M) = \rho_m(0) - aM^2$, except very close to T_c.[3]

[3]This relation cannot hold very close to T_c because of the influence of the spin-spin correlation on the resistivity, due to which there is a temperature-dependent change in the zero-field magnetic resistivity even above T_c (see inset to Fig. A.1 and Refs. [60, 20]). We estimated the contribution of this effect to the resistivity by integration of the diverging part of $d\rho/dT$. This contribution is found

Based on this result and using measurements of resistivity and magnetoresistance we determined the values of the parameters β, γ, and C^+/C^- which describe the magnetic critical behavior in $SrRuO_3$. From the zero-field resistivity data we determined that $\beta = 0.34 \pm 0.02$. From the magnetoresistance data below T_c we found that $\gamma = 1.14 \pm 0.07$, and using the data above T_c we found that $\gamma = 1.17 \pm 0.14$. The consistency of values of γ obtained below and above T_c supports the validity of our analysis. Comparing the susceptibilities above and below T_c we obtained $C^+/C^- \sim 4$.

Studying the magnetic phase transition in thin films via transport measurements has special advantages relative to bulk measurements of magnetization that suffer from weak signals on top of large contribution of the substrate (which is temperature and field dependent).

The current results are somewhat different from the ones presented in a previous report on the critical indices which relied on direct measurements of magnetization [34]. While the zero-field resistivity below T_c gives a similar result for β, we obtain a different value for γ above T_c (which is determined from field-dependent measurements). We attribute the difference mainly to the fact that previously the field was not applied along the easy axis and therefore unwanted changes in the direction of the magnetic moment were involved.

In Table A.1 we compare the extracted critical exponents with the exponents of the different models (mean-field, Ising, Heisenberg). The comparison suggests that $SrRuO_3$ belongs to Ising universality class. This result can be understood in view of

---

to be small relative to the resistivity changes considered in our analysis, and its changes become less and less significant when departing from T_c. As mentioned previously, we excluded from our analyzes temperatures which are too close to T_c.

	β	γ $(T < T_c)$	γ $(T > T_c)$	C^+/C^-
Mean field theory	0.5	1	1	2
3d Ising model (Ref. [57])	0.326	1.24	1.24	4.8
3d Heisenberg model (Ref. [58])	0.36	1.39	1.39	
$SrRuO_3$ (this work)	0.34 ± 0.02	1.14 ± 0.07	1.17 ± 0.14	~ 4

Table A.1: Comparison of critical parameters of $SrRuO_3$ with different models.

the high uniaxial anisotropy of $SrRuO_3$. Later this result has been confirmed by the fact that the susceptibility diverges at T_c only along one crystallographic direction, as described in Chapter 4.

In conclusion, the consistent picture of the ferromagnetic phase transition not only supports the obtained values of the critical exponents, but it also reinforces the simple relation between the magnetic resistivity and the magnetization: $\rho_m(M) = \rho_m(0) - aM^2$, which holds for a surprisingly wide range of M.

A.4 Discussion of criticism

After these results on Ising critical behavior in $SrRuO_3$ *films* were published (in Ref. [61]), Kim *et al.* investigated the critical behavior in $SrRuO_3$ *crystals* [62], and reached different conclusions. Ising exponent for the specific heat was obtained, but mean-field exponents were found for the magnetization. To resolve the inconsistency, the authors re-analyzed the specific heat data, and fitted them to mean-field behavior with Gaussian fluctuations of XY-type spins, thus obtaining a self-consistent picture of the phase transition, in which the transition is dominated by mean-field behavior down to a very close vicinity of T_c. Kim *et al.* suggested that our results from films did not represent the true critical behavior because our data were taken farther from T_c, and because the films were less homogeneous (based on a greater smearing of the phase transition).

However, our work presented here in Chapter 4 implies, based on the behavior of the paramagnetic susceptibility, that:

1. The real critical behavior (at least in the films) is Ising (because the susceptibility diverges only along one direction). Crossover through XY fluctuations is not an option, since $\chi_a \simeq \chi_c \ll \chi_b$.

2. The critical range in $SrRuO_3$ is not very small (as suggested by Kim *et al.*), but relatively large: χ_b is 5 times greater than χ_a and χ_c already at $t = 0.1$. Therefore, our critical behavior data (which are centered around $t \simeq 0.05$) are well inside the critical range. Furthermore, the difference between the results of Kim *et al.* and our results is unlikely to be due to measurements out of

the critical range, since it is unlikely to obtain mean-field-like behavior (their results) in a crossover between Ising-like exponents (obtained by us) and true Ising behavior (implied by Chapter 4).

Therefore, a different reason should be sought to explain the difference between the results in films and in crystals.

There is a reason to suspect that the crystals studied in Ref. [62] are twinned (include several orientations): Kim *et al.* report a low-temperature magnetic moment of $1.1\mu_B$ per Ru, compared to $1.4\mu_B$ per Ru found in single-oriented films. If the crystals were indeed twinned, the macroscopic behavior of the magnetization would not be the intrinsic one, but averaged upon regions with the different orientations; **H** would not be collinear with the easy axis (at least not for all the orientations) and the resulting angle between **H** and **M** would change as a function of magnetization and magnetic field values, and would be, in general, different for the different orientations. This could significantly bias the critical behavior fits.

Another possibility is that the difference in the behavior of films and crystals is real, and it is related to small differences in the lattice structure between them (since the films are slightly strained by the substrate), which is also creating the 8% difference in T_c [29].

Appendix B

List of Publications

Domain wall resistivity in $SrRuO_3$
L. Klein, Y. Kats, A. F. Marshall, J. W. Reiner, T. H. Geballe, M. R. Beasley, and A. Kapitulnik, Phys. Rev. Lett. **84**, 6090 (2000).

Domain wall resistivity in $SrRuO_3$: the influence of domain walls spacing
L. Klein, Y. Kats, A. F. Marshall, J. W. Reiner, T. H. Geballe, M. R. Beasley, and A. Kapitulnik, in *Proceedings of ICM2000*, J. Magn. Magn. Mater. **226**, 780 (2001).

Magnetic resistivity in $SrRuO_3$ and the ferromagnetic phase transition
Y. Kats, L. Klein, J. W. Reiner, T. H. Geballe, M. R. Beasley, and A. Kapitulnik, Phys. Rev. B **63**, 054435 (2001).

Negative deviations from Matthiessen's rule in $SrRuO_3$ and $CaRuO_3$
L. Klein, Y. Kats, N. Wiser, M. Konczykowski, J. W. Reiner, T. H. Geballe, M. R. Beasley, and A. Kapitulnik, Europhys. Lett. **55**, 532 (2001).

Can fractional power-law conductivity explain the deviations from Matthiessen's rule in $SrRuO_3$?
Y. Kats and L. Klein, in *Proceedings of SCES2001*, Physica B **312-313**, 793 (2002).

Magnetoresistance scaling in $BaRuO_3$
S. Levy, Y. Kats, M. K. Lee, C. B. Eom, and L. Klein, in *Proceedings of SCES2001*, Physica B **312-313**, 795 (2002).

Frenet algorithm for simulations of fluctuating continuous elastic filaments
Y. Kats, D. A. Kessler, and Y. Rabin, Phys. Rev. E **65**, 020801 (2002).

Paramagnetic anisotropic magnetoresistance in thin films of $SrRuO_3$
I. Genish, Y. Kats, L. Klein, J. W. Reiner, and M. R. Beasley, in *Proceedings of 9th Joint MMM-Intermag Conference*, J. Appl. Phys. **95**, 6681 (2004).

Large anisotropy in the paramagnetic susceptibility of $SrRuO_3$ films
Y. Kats, I. Genish, L. Klein, J. W. Reiner, and M. R. Beasley (submitted); e-print: cond-mat/0311341.

Testing the Berry phase model for extraordinary Hall effect in $SrRuO_3$
Y. Kats, I. Genish, L. Klein, J. W. Reiner, and M. R. Beasley (submitted); e-print: cond-mat/0405645.

Comment on "Scaling of the anomalous Hall effect in $Sr_{1-x}Ca_xRuO_3$"
Y. Kats and L. Klein (submitted).

Local measurements of magnetization reversal in thin films of $SrRuO_3$
I. Genish, Y. Kats, L. Klein, J. W. Reiner, and M. R. Beasley (submitted).

Bibliography

[1] J. Smit, Physica **24**, 39 (1958).

[2] L. Berger, Phys. Rev. B **2**, 4559 (1970).

[3] M. V. Berry, Proc. R. Soc. Lond. A **392**, 45 (1984).

[4] T. Jungwirth, Q. Niu, and A. H. MacDonald, Phys. Rev. Lett. **88**, 207208 (2002).

[5] Z. Fang *et al.*, Science **302**, 92 (2003).

[6] Y. Yao *et al.*, Phys. Rev. Lett. **92**, 037204 (2004).

[7] G. Sundaram and Q. Niu, Phys. Rev. B **59**, 14915 (1999).

[8] R. Karplus and J. M. Luttinger, Phys. Rev. **95**, 1154 (1954).

[9] J. M. Luttinger, Phys. Rev. **112**, 739 (1958).

[10] M.-C. Chang and Q. Niu, Phys. Rev. Lett. **75**, 1348 (1995).

[11] J. Ye *et al.*, Phys. Rev. Lett. **83**, 3737 (1999); Y. Taguchi *et al.*, Science **291**, 2573 (2001); R. Shindou and N. Nagaosa, Phys. Rev. Lett. **87**, 116801 (2001).

[12] J. E. Hirsch, Phys. Rev. B **60**, 14787 (1999).

[13] R. J. Bouchard and J. L. Gillson, Mater. Res. Bull. **7**, 873 (1972).

[14] C. B. Eom *et al.*, Science **258**, 1766 (1992).

[15] C. B. Eom *et al.*, Appl. Phys. Lett. **63**, 2570 (1993).

[16] W. Bensch, H. W. Schmalle, and A. Reller, Solid State Ionics **43**, 171 (1990).

[17] B. J. Kennedy, B. A. Hunter, and J. R. Hester, Phys. Rev. B **65**, 224103 (2002).

[18] Q. Gan *et al.*, J. Appl. Phys. **85**, 5297 (1999).

[19] P. B. Allen *et al.*, Phys. Rev. B **53**, 4393 (1996).

[20] L. Klein *et al.*, Phys. Rev. Lett. **77**, 2774 (1996).

[21] P. Kostic *et al.*, Phys. Rev. Lett. **81**, 2498 (1998).

[22] J. S. Dodge *et al.*, Phys. Rev. Lett. **85**, 4932 (2000).

[23] L. Klein *et al.*, Europhys. Lett. **55**, 532 (2001).

[24] Y. Kats and L. Klein, Physica B **312-313**, 793 (2002).

[25] A. P. Mackenzie *et al.*, Phys. Rev. B **58**, R13318 (1998).

[26] D. J. Singh, J. Appl. Phys. **79**, 4818 (1996).

[27] I. I. Mazin and D. J. Singh, Phys. Rev. B **56**, 2556 (1997).

[28] G. Santi and T. Jarlborg, J. Phys.: Condens. Matter **9**, 9563 (1997).

[29] Q. Gan *et al.*, Appl. Phys. Lett. **72**, 978 (1998).

[30] D. C. Worledge and T. H. Geballe, Phys. Rev. Lett. **85**, 5182 (2000); B. Nadgorny *et al.*, Appl. Phys. Lett. **82**, 427 (2003); P. Raychaudhuri *et al.*, Phys. Rev. B **67**, 020411(R) (2003).

[31] V. Korenman, J. L. Murray, and R. E. Prange, Phys. Rev. B **16**, 4032 (1977); V. Korenman and R. E. Prange, Phys. Rev. Lett. **53**, 186 (1984).

[32] J. S. Dodge *et al.*, Phys. Rev. B **60**, R6987 (1999).

[33] A. F. Marshall *et al.*, J. Appl. Phys. **85**, 4131 (1999).

[34] L. Klein *et al.*, J. Phys.: Condens. Matter **8**, 10111 (1996).

[35] J. W. Reiner, Ph. D. thesis, Stanford University (2002).

[36] Y. Kats *et al.* (submitted); e-print: cond-mat/0311341.

[37] C. D. Graham, Jr., Phys. Rev. **112**, 1117 (1958).

[38] R. M. Bozorth, *Ferromagnetism* (Van Nostrand, New York, 1951), p. 569.

[39] D. Weller *et al.*, Phys. Rev. Lett. **72**, 2097 (1994).

[40] J. S. Griffith, *The Theory of Transition-Metal Ions* (Cambridge University Press, Cambridge, 1971), p. 437-439.

[41] I. Genish *et al.*, J. Appl. Phys. **95**, 6681 (2004).

[42] L. Klein *et al.* (unpublished).

[43] M. Izumi *et al.*, J. Phys. Soc. Jpn. **66**, 3893 (1997).

[44] L. Klein *et al.*, Phys. Rev. B **61**, R7842 (2000).

[45] R. A. Rao, Q. Gan, and C. B. Eom, Appl. Phys. Lett. **71**, 1171 (1997).

[46] R. J. Kennedy, R. Madden, and P. A. Stampe, J. Phys. D: Appl. Phys. **34**, 1853 (2001).

[47] S. J. Benerofe *et al.*, J. Vac. Sci. Technol. B **12**, 1217 (1994).

[48] R. Mathieu *et al.*, Phys. Rev. Lett. **93**, 016602 (2004).

[49] C. Kittel, *Introduction to Solid State Physics* (Wiley, 1986), p. 450.

[50] H. B. Callen and E. Callen, J. Phys. Chem. Solids **27**, 1271 (1966).

[51] P. Pfeuty and G. Toulouse, *Introduction to the Renormalization Group and to Critical Phenomena* (Wiley, 1977), Chapter 8.

[52] G. Cao *et al.*, Phys. Rev. B **56**, 321 (1997).

[53] H. Suzuki and T. Watanabe, J. Phys. Soc. Jpn. **30**, 367 (1971).

[54] P. J. Jensen *et al.*, Phys. Rev. B **67**, 184417 (2003).

[55] L. Klein *et al.*, Phys. Rev. Lett. **84**, 6090 (2000).

[56] H. Eugene Stanley, *Introduction to Phase Transitions and Critical Phenomena,* (Oxford University Press, New York, 1971), pp. 46-47.

[57] M. Campostrini *et al.*, Phys. Rev. E **60**, 3526 (1999).

[58] C. Holm and W. Janke, Phys. Rev. B **48**, 936 (1993).

[59] M. Seeger *et al.*, Phys. Rev. B **51**, 12585 (1995).

[60] M. E. Fisher and J. S. Langer, Phys. Rev. Lett. **20**, 665 (1968).

[61] Y. Kats *et al.*, Phys. Rev. B **63**, 054435 (2001).

[62] D. Kim *et al.*, Phys. Rev. B **67**, 100406 (2003).